Spatial and Temporal Variation of Satellite Ocean Color in the Eastern Indian Ocean

December 2005

Graduate School of Science and Technology

Nagasaki University

TAN CHUN KNEE

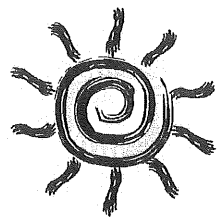

TO MY FAMILY

SWEE SWEE

YAN JUN

YAN HONG

Abstract

The eastern Indian Ocean region is generally influenced by the Asian monsoon system. Due to lack of data and constrains of in situ observation, the oceanographic condition in this region is unclear. This research is aimed at studying the seasonal and interannual chlorophyll a (chl a) variation in the eastern Indian Ocean, and further assessed the 2004 tsunami effects on the marine environment in the region. The research work had been divided into three major sections. The first section was focused on studying the influences of Asian monsoon on the seasonal chl a variation in Malacca Straits (MS) using Sea-viewing Wide Field-of-view Sensor (SeaWiFS) data. The second section was the investigation of interannual chl a variation during northeast monsoon (NEM) in the Southeastern Bay of Bengal (SEBOB) using SeaWiFS ocean color data. The last section included application of Moderate Resolution Imaging Spectroradiometer (MODIS) Aqua ocean color data to assess the 2004 Indian Ocean tsunami effects on the chl a and turbidity variation.

Results showed that chl *a* in MS experienced seasonal variability. At northern MS, SeaWiFS chl a increased as much as twice during NEM compared to southwest monsoon (SWM). At the southern MS, SeaWiFS OC4 algorithm was found over-estimating chl a in the areas of high normalized water leaving radiance at 555 nm value (nLw 555). Strong correlation between the nLw 555 and suspended sediment (SS) concentration suggested that high turbidity could contribute to the over-estimation of SeaWiFS chl a. Monsoon wind strongly influenced the spatial distribution and seasonal variation of the chl a at northern MS. During NEM, bloom of phytoplankton started from eastern MS, and it was advected towards Andaman Sea by northeasterlies. NEM wind created positive wind stress curl along 4.5°N to 6.5°N in the Straits, which caused positive Ekman pumping resulting upwelling. Consequently, upwelling helped in replenish of the surface water nutrients. Thus, maintaining the phytoplankton bloom over the continental shelf. Low chl a was observed during SWM, and this was attributed to negative wind stress curl and downwelling. The unique topology of

MS, where the mountain ranges at Malay Peninsular and Sumatra Island act as the monsoon windshield, enable the occurrence of both upwelling and downwelling in the northern MS during different monsoon periods.

The first section describes the fundamental knowledge of the seasonal chl a variation in the study area. With this information, we further extended the spatial and temporal limit of the study to the whole SEBOB that include Indian Ocean, Bay of Bengal (BOB), Andaman Sea and MS. The interannual chl a variation at SEBOB during NEM was found closely related to the variation of wind and sea surface height anomaly (SSH) as the result of large ocean-atmospheric events in both Indian and Pacific Ocean. During Indian Ocean Dipole (IOD) 1997 – 98, anomalous alongshore wind driven upwelling caused large chl a bloom along the western Sumatra. Another bloom occurred later at the northwestern Sumatra (NWS) and was related to the lowering of SSH by Rossby wave propagation. In situ observation showed the lifting of thermocline within the low SSH Rossby wave that indicating the nutrient entrainment to the surface layer. After the Rossby wave passage, high chl a at NWS could be attributed to the cyclonic eddy that continues supplying nutrients to the surface water. Higher chl a variation in MS compared to that in NWS could be due to the shallower depth in the straits. Chl a variation in the northern MS was closely related to NEM wind. During NEM 1998 – 99, lower chl a in MS could be due to the El Niño-Southern Oscillation (ENSO) related weaker monsoon wind and higher SSH after IOD. Based on the results of this study, a detail investigation on the relationship of surface current, eddy system and planetary wave on chl a is necessary for a better understanding of the spatial chl a variation in SEBOB.

The 2004 Indian Ocean tsunami had been reported causing vast destruction on marine environment; however its effects on the primary production and upwelling event was unknown. Chl a and nLw 551 before and after the tsunami event were processed using SeaWiFS Data Analysis System (SeaDAS) and the variations were examined in the third section. Results showed that high sedimentation caused by the backwash resulted in over-

estimation of the chl a values. However, the chl a concentration in the upwelling area at northern MS did not exhibit any significant changes by the tsunami. The chl a bloom in this upwelling area was mainly driven by the northeast monsoon wind. At the seriously eroded coastline along western Sumatra, continuous sedimentation was observed.

This study has proven the effectiveness of ocean color remote sensing in providing synoptic and comprehensive monitoring of the oceanographic conditions. It also demonstrated the ocean color remote sensing as a useful tool for assessing the tsunami effects. The findings of this study in the eastern Indian Ocean region is expected to increase the effectiveness of the marine resources and coastal zone management. We suggested that long term monitoring of marine environment should be carried out using the combination of remote sensing and in situ study.

Acknowledgements

I extend my sincere gratitude and appreciation to many people who made this PhD thesis possible. With a deep sense of gratitude, I wish to express my sincere thanks to my supervisors, Professor Joji Ishizaka whose help, stimulating suggestions, and encouragement helped me in all the time of research for and writing of this thesis. The appreciation also goes to Prof. Hideaki Nakata and Assoc. Prof. Akihide Tada for reading the thesis and useful comments for the improvement of this work.

I specially thank Dr. Atsuyoshi Manda, Dr. N. H. Saji, and Dr L. C. Quah for their help extended to me when I approached them and the valuable discussion that I had with them. Special thanks are due to Dr. A. Tanaka and Dr. H. Sasaki for guidance and comment in the research. Many thanks to Dr. Helen. Marcial, Dr. M. V. Grageda, Tomas Gonzales, and Dr. Sarat C. Tripathy for looking closely at the English style and grammar of this thesis, correcting both and offering suggestions for improvement.

I would like to express my gratitude to Prof. A. Kawamura, Dr. Takaya Namba, and Prof. Dr. Capt. Mohd. Ibrahim Hj. Mohamed for their encouragement and help during my PhD application to Japan. I thank all the cruise members and scientists that assisted my research during the MASDEC Cruise 5 on the K.L. Cermin. Thanks to Mr. Galil and his room mate from Sudan for their hospitality during my home stay with them in Serdang, Malaysia.

I would also like to acknowledge with much appreciation of the support from Prof. Mery Jane Perry from University of Maine that enable me to attend the summer course in Darling Marine Center. Special acknowledgement to IOCCG for supporting my attendance to the international conference at Halifax, Canada.

The episode of acknowledgement would not be complete without the mention of the senior and lab mate at Ishizaka Laboratory, Mrs. Yamada Keiko, Mr. Eko Siswanto, Ms. Wakamatsu Ai, and the undergraduate students.

I am grateful to my wife Swee Lee for the inspiration and moral support she provided throughout my research work and her patience was tested to the utmost by a long period of separation. Without her loving support and understanding I would never have completed my present work. Particularly, I owe to my children Yan Jun and Yan Hong for their silent prayer for my work at the time when they needed my company most.

Finally, I would like to thank all whose direct and indirect support helped me completing my thesis in time.

List of Figures

List of Abbreviations

Abbreviation	Description
ARGO	Array for Real-time Geostrophic Oceanography
AVISO	Archiving, Validation and Interpretation of Satellite Oceanographic data
BOB	Bay of Bengal
CDOM	Colored dissolve organic matter
COCTS	Chinese Ocean Color and Temperature Sensor
CORDIO	Coral Reef Degradation in the Indian Ocean
CZCS	Coastal Zone Colour Scanner
Chl a	Chlorophyll a
DAAC	Distributed Active Archive Center
DMI	Dipole Mode Index
EC	Equatorial Current
ENSO	El Niño-Southern Oscillation
EP	Ekman pumping
FNMOC	Fleet Numerical Meteorology and Oceanography Center
FRSGC	Frontier Research System for Global Change
GIS	Geographical Information System
GLI	Global Imager
GOCI	Geostationary Ocean Colour Imager
GODAE	Global Ocean Data Assimilation Experiment
IOD	Indian Ocean Dipole
MASDEC	Malacca Straits Research and Development Centre
MERIS	Medium Resolution Imaging Spectrometer
MODIS	Moderate Resolution Imaging Spectroradiometer
MOS	Modular Optical Scanner
MS	Malacca Straits
NASA	National Aeronautics and Space Administration
NCEP	National Centers for Environmental Prediction
NEC	North Equatorial Current
NECC	North Equatorial Counter Current
NEM	Northeast monsoon
nLw	normalized water leaving radiance
NOAA	National Oceanic and Atmospheric Administration
NVODS	National Virtual Ocean Data System
NWS	Northwestern Sumatra
OCM	Ocean Color Monitor
OCTS	Ocean Color and Temperature Sensor
ODV	Ocean Data View
PDC	Pacific Disaster Center
PFEL	Pacific Fisheries Environmental Laboratory
RGB	Red, Green, Blue
SEAFDEC	Southeast Asian Fisheries Development Center
SEBOB	Southeastern Bay of Bengal
SOI	Southern Oscillation Index
SS	Suspended sediment
SSH	Sea Surface Height Anomaly
SST	Sea surface temperature
SWM	Southwest monsoon

SeaDAS	SeaWiFS Data Analysis System
SeaWiFS	Sea-viewing Wide Field of view Sensor
TOVAS	TRMM Online Visualization and Analysis System
TRMM	Tropical Rainfall Measuring Mission
UNEP	United Nation Environment Programme
VIIRS	Visible/ Infrared Imager/Radiometer Suite
WC	Wind stress curl
WS	Wind speed

Contents

Chapter 1. General Introduction

1.1 Background of eastern Indian Ocean

The Indian Ocean is the third-largest ocean in the world, covering about 20% of the Earth's water surface. It is bounded on the north by southern Asia; on the west by the Arabian Peninsula and Africa; on the east by the Malay Peninsula, the Sunda Islands, and Australia; and on the south by the Southern Ocean. This ocean is nearly 10,000 km wide at the southern tips of Africa and Australia; its area is 73,556,000 km^2, including the Red Sea and the Persian Gulf. The ocean's volume is estimated to be 292,131,000 km^3 (Wikipedia, 2005B).

On 26 December 2004, the second largest earthquake hit the eastern Indian Ocean (Stein and Okal, 2005). The earthquake and tsunami disaster 2004 has brought the world attention to this region. The major waters bodies at the eastern Indian Ocean consist of Malacca Straits (MS), Andaman Sea and Bay of Bengal (BOB). All these areas are strongly influence by the seasonal reversing wind, called "monsoon".

Monsoonal climate dominates the northern Indian Ocean, and its effects are felt far into the subtropics of the Southern hemisphere (Tomczak and Godfrey, 2002). The word "monsoon" is derived from the Arabic word "mausim" which means season (Malaysian Meteorological Service, 2005). Monsoon is caused by land-sea temperature differences due to heating by the sun's radiation. The Asian monsoon system is characterized by two monsoon regimes, namely, the southwest monsoon (SWM) from late May to September, and the

northeast monsoon (NEM) from November to March (Malaysian Meteorological Service, 2005).

The NEM is characterized by high pressure over the Asian landmass and northeasterly winds over the tropics and northern subtropics (Tomczak and Godfrey, 2002). In winter, the continental landmass cools rapidly resulting in extremely low temperatures over central Asia. As temperature drops, atmospheric pressure rises and an intense high pressure system (anticyclone) develops over Siberia. Cold air flows out of Siberia as northwesterlies and turns into northeasterlies on reaching the coastal waters of China before heading towards Southeast Asia (Malaysian Meteorological Service, 2005). NEM monsoon caused high rainfall at the Vietnam, east coast of Malay Peninsular and Indonesia regions.

During the SWM, a deep heat low develops over northern Arabia and Pakistan. The Australia heat low of the southern summer is replaced by a center of high pressure. The SWM brings heavy rainfall to most parts of the Indian subcontinent, Burma and Thailand. Intense summer storms can have a strong impacts on the Indian Ocean (Church et al., 1998). The fresh water input from Ganges and Brahmaputra and several peninsular Indian rivers influences estuaries characteristics with reduced surface salinities over most part of the BOB (Ittekkot *et al.*, 2003).

1.1.1 Bay of Bengal

Bay of Bengal, a northern extended arm of the Indian Ocean, is located between

latitudes 5°N and 22°N and longitudes 80°E and 100°E. It resembles a triangle in shape, and it is bounded in the west by the east coasts of Sri Lanka and India, on the north by the deltaic region of the Ganges-Brahmaputra-Meghna river system, and on the east by the Myanmar peninsula extended up to the Andaman-Nicobar ridges (Banglapedia, 2005). The southern boundary of the Bay is approximately along the line drawn from Dondra Head in the south of Sri Lanka to the north tip of Sumatra. The Bay occupies an area of about 2,200,000 km^2 and the average depth is 2,600 m with a maximum depth of 5,258 m (Banglapedia, 2005).

Many major rivers of India flow west to east into the BOB: in the north, the Ganges River (or Ganga), Meghna and Brahmaputra rivers, and in the south Mahanadi, Godavari, Krishna and Kaveri (sometimes written as Cauvery) rivers. The Irrawaddy River of Burma also flows into the bay. Fresh water from the rivers largely influences the coastal northern part of the Bay. The River of Bangladesh discharges the vast amount of 1,222,000,000 m^3 of fresh water into the Bay. In the coastal region of the Bay and in the northeastern part of the Andaman Sea where a significant influence of river water is present, the temperature and salinity are seen to be different from the open part of the Bay. The temperature, salinity and density of the water of the southern part of the BOB is, almost the same as in the open part of the ocean (Banglapedia, 2005).

Surface circulation at BOB is found to be generally clockwise from January to July and counter-clockwise from August to December, in accordance with the reversible monsoon wind systems. An important vertical circulation in the BOB is upwelling. In this process,

sub-surface water is brought toward the surface, and conversely a downward displacement is called downwelling or sinking. Upwelling and downwelling are seasonal. The persistence of the monsoon, especially from the southwest and the orientation of the coasts cause upwelling to occur along most of the east coast of India. In the east coast of India the upwelling takes place in summer and down welling in winter, and in the eastern part of the BOB and in the Myanmar coast, upwelling occurs in winter and the downwelling in summer (Banglapedia, 2005).

1.1.2 Andaman Sea

Andaman Sea is the body of water in the northeastern corner of the Indian Ocean that lies to the west of the Malay Peninsula, the north of Sumatra, the east of the Andaman Islands, and the south of the Irrawaddy Delta in Burma. It is roughly 1200 km long (north-south) and 650 km wide (east-west), with an area of 797700 km^2. Its average depth is 870 m, and the maximum depth is 3777 m (Wikipedia, 2005A). On the west of Andaman Sea is bounded by the chain of Andaman and Nicobar Archipelagoes, which permit restricted communication between it and the BOB (Satish and Gouveia, 1998). The surface salinities exhibit strong seasonal variations due to an extremely large freshwater influx from the Irrawaddy and Salween rivers during monsoon season.

The northern Andaman Sea is influence by oceanic water characteristic, while the southern strecth is dominated by coastal water characteristic. At the northern Andaman Sea,

the surface current shows clockwise circulation; while at the southern, counter-clockwise circulation was observed. Both circulations are predominant in both NEM and SWM. The intersection of these two circulations initiates a mixing zone between the oceanic and coastal waters around southwest of Phuket (Limpsaichol, 2005).

High productivity at the shelf break areas during the NEM might be attributed to upwelling or internal wave action (Limpsaichol, 2005). Yesaki and Jantrarapagdee (1981) found that during NEM, Andaman Sea deep water ascended to above the shelf. The subsurface temperature of 25°C located at the shelf edge at about 75 m in December further ascended to less than 50 m in March. The findings indicate upwelling of deep water mass during NEM. During SWM, the 25°C water mass normally descended to about 100 m.

1.1.3 Malacca Straits

The MS is located between the east coast of Sumatra Island in Indonesia and the west coast of Peninsular Malaysia, and is linked with the Strait of Singapore at its southeast end. The MS are bordered by four littoral States, namely Thailand, Indonesia, Malaysia and Singapore. The length is around 1100 km, with the widest section (400 km) near the northwest entrance, narrowing gradually to around 15 km at the southeast entrance near the Riau Archipelago.

The depth of the water is irregular, from 17 to 55 m (Chua, 2000). The topography in MS varies between the northern and southern areas. Depth of the water is deeper at the

northern than at the southern parts. Sudden decrease of depth around One Fathom Bank creates a physical barrier for the water exchange between the north and south (Liong, 1974).

Currents follow the topographic configuration of the sea bottom. The flow of surface current is stronger during the northeast Monsoon when the dominant direction of the surface current is from the South China Sea to the Andaman Sea (Chua, 2000). Surface current also enters from the Andaman Sea but turns northwest of Pulau Penang and the Perak coast. There is an undercurrent owing from the Andaman Sea towards the Straits during monsoon periods, which causes a light upwelling near the One Fathom Bank (Uktolseya, 1988).

The hydrographic and ecological features of the Straits are greatly influenced by the Adaman Sea and the South China Sea as well as the drainage from the river systems of Peninsular Malaysia and Sumatra. As a result, the Straits of Malacca presents a unique estuarine environment with fairly rich primary productivity supporting substantial aquatic renewable resources, which become a significant source of food sustenance and employment to the coastal population (Chua, 2000).

From an economic and strategic perspective the MS is one of the most important shipping lanes in the world, an equivalent of the Suez Canal, or the Panama Canal. The Strait forms the main ship passageway between the Indian Ocean and the Pacific Ocean, linking three of the world's most populous nations: India, Indonesia and China (Wikipedia, 2005C). The Strait carries 50,000 vessels per year, carrying between one-fifth and one quarter of the world's sea trade. All these factors have caused the area to become a target for piracy and a

perceived target for terrorism. If the terrorist attack occurred, it would have a devastating effect on world trade (Wikipedia, 2005C). Another shipping risk in the Straits is the yearly haze that persists due to raging bush fires in Sumatra. The haze can literally choke shipping by reducing visibility to as low as 200 m making navigation in such a narrow and busy trade route hazardous (Wikipedia, 2005C).

1.2 Ocean Color Remote Sensing

Of all the techniques used in ocean remote sensing, the observation of ocean color from satellite is perhaps the most easily understood in concept, because it is the most similar to our own personal remote sensing device – the human eyes (Robison, 2004). In the nineteenth and early twentieth centuries, the first oceanographers sought to use ocean color as an indicator of water masses and indirectly of ocean currents. They began to record the color of seawater in a qualitative but objective manner using the Forel Scale (Fairbridge, 1966) and to quantify a measure of its transparency using the Secchi disk (Secchi, 1866).

The "colour" of the ocean is determined by the interactions of incident light with substances or particles present in the water. The most significant constituents are free-floating photosynthetic organisms (phytoplankton) and inorganic particulates. Phytoplankton contains chlorophyll, which absorbs light at blue and red wavelengths and transmits in the green. Particulate matter can reflect and absorb light, which reduces the clarity (light transmission) of the water. Substances dissolved in water can also affect its colour (IOCCG, 1999).

In the ocean, light reflects off particulate matter suspended in the water, and absorption is primarily due to the photosynthetic pigments (chlorophyll) present in phytoplankton. The net result of these optical interactions is light radiating from the ocean surface - the water-leaving radiance. Radiometers are instruments that measure the radiance intensity at a given wavelength of light. The measured radiance may then be quantitatively related to various constituents in the water column that interact with visible light, such as chlorophyll. The concentration of chlorophyll, in turn, may be used to calculate the amount of carbon being produced by photosynthesis, which is termed primary productivity (IOCCG, 1999).

The chlorophyll a (chl a) has been used as the relative measurement to phytoplankton abundance and biomass in the ocean (Martin, 2004). The goal of remote sensing of ocean colour is to derive quantitative information on the types of substances present in the water and on their concentrations, from variations in the spectral form and magnitude of the ocean colour signal. A primary goal of ocean colour remote sensing is to produce synoptic fields of chlorophyll pigment, an index of phytoplankton biomass.

1.2.1 Classification of marine waters

In the ocean color research, the marine waters are classified into oceanic water (Case 1) and turbid water (Case 2). In the Case 1 water, all of the optical properties in the ocean are determined by the phytoplankton; in Case 2 water, they are determined by various factors,

such as suspended sediment, colored dissolve organic matter (CDOM) and phytoplankton concentration (Acker, 2005).

Case 1 waters are those waters in which phytoplankton are the principle agents responsible for the variations in optical properties of the waters. Case 1 water covered about 90% of the world ocean. Their optical properties are simpler, easier to analyse, model and derived the geophysical parameters. Case 2 waters are influence not just by phytoplankton, but also other substances, that vary independently of phytoplankton, notably inorganic particles in suspension and yellow substance (IOCCG, 2000).

Although it covered about 10% of the world ocean, but the Case 2 waters support 60% of the world population and 90% of the world marine fish catch. Complexity in the optical properties makes it difficult to quantify the geophysical values. Besides, the relationship between ocean colour and the constituents of the water may vary regionally or seasonally, according to the composition of algal species, size distribution of phytoplankton cells, mineral composition of the inorganic particles in suspension or the chemical composition of dissolved organic substances (IOCCG, 2000).

1.2.2 Ocean color sensors

The first instrument to collect scientific data on the colour of the ocean was the Coastal Zone Colour Scanner (CZCS), an instrument on the NIMBUS-7 satellite, which operated from November 1978 to June 1986. The CZCS had very modest spectral resolution

and a modest goal of estimating a phytoplankton pigment index. The CZCS was more to an experimental and proof-of-concept mission. The next instruments were the Japanese Ocean Color and Temperature Sensor (OCTS) on the ADEOS-1 satellite that operated from August 1996 to June 1997, and the German Modular Optical Scanner (MOS) launched in 1996 on the Indian Remote Sensing Satellite IRS-P3.

The Sea-viewing Wide Field of view Sensor (SeaWiFS) ocean color sensor was launched in August 1997 and continuously provided almost 8 years of global bio-optical data since September 1997. SeaWiFS has been the most successful among ocean color mission where the sensor still operating until present. Moderate Resolution Imaging Spectroradiometer (MODIS) was launched on Terra in December 1999 and on Aqua in May 2002. Both SeaWiFS and MODIS imagery has been applied extensively until operational level, which are the most important ocean color sensors to date.

Other ocean color satellites and instrument include the following. In 1999, the German Ocean Color Monitor (OCM) was launched on the Indian IRS-P4. In March 2002, the European Medium Resolution Imaging Spectrometer (MERIS) was launched on ENVISAT. In May 2002, the Chinese Ocean Color and Temperature Sensor (COCTS) was launched on the Haiyang-1 satellite. In December 2002, Japan launched the Global Imager (GLI) on the ADEOS-2 satellite, however ADEOS-2 failed in October 2003. Some new sensors are scheduled to be launching in the near future, eg. Visible/ Infrared Imager/Radiometer Suite (VIIRS) on NPP (2006) and NPOESS (2009) by NASA/IPO, and a

stationary ocean color satellite Geostationary Ocean Colour Imager (GOCI) on COMS-1 by South Korea in 2008.

1.3 Previous study about phytoplankton distribution at eastern Indian Ocean

Previous study of ocean color in Indian Ocean is mainly focused on the western Indian Ocean. Arabian Sea is one of the world's most productive regions of the ocean. This is brought about through a range of physical processes; for example, the coastal upwelling along Somalia, Arabia and southern part of the west coast of India turns the coastal waters into a region of high biological productivity. The open ocean upwelling (Bauer *et al.*, 1991; Brock *et al.*, 1991), wind-driven mixing (McCreary *et al.*, 1996; Lee *et al.*, 2000) and lateral advection (Young and Kindle, 1994; Prasanna Kumar *et al.*, 2001) makes the open ocean waters of the central Arabian Sea more productive. Phytoplankton blooms of lesser intensity are also known to occur along the west coast of India during summer monsoon (Lierheimer and Banse, 2002) as a result of coastal upwelling (Shetye *et al.*, 1990; McCreary *et al.*, 1996).

Relatively, the phytoplankton variations at the eastern part of the Indian Ocean was unclear, and this may be attributed to the inadequate coverage by the CZCS which helped in the early detection of the chl a blooms of the Arabian Sea (Vinayachandran *et al.*, 2004). Shipboard observations off the east coast of India and along 88°E suggest that the primary productivity in the Bay of Bengal is considerably lower than that in the Arabian Sea (Gomes *et al.*, 2000; Kumar *et al.*, 2002; Madhupratap *et al.*, 2003). By using the OCTS and SeaWiFS

imagery, Vinayachandran and Mathew (2003) show that there is a phytoplankton bloom caused by open ocean upwelling that driven by Ekman pumping (EP) in the southwestern part of BOB during NEM. They further found that the cyclone during NEM causing intense bloom at the western BOB. During SWM, Vinayachandran *et al.* (2004) found there is chl a bloom at the southern coast of Sri Lanka caused by the open ocean upwelling associated with the Sri Lanka Dome. Prasanna Kumar *et al.* (2004) suggested that cold core eddies could possibly act as the mechanism of nutrient injection to the oligotrophic waters in the BOB during summer.

Along the coast of south Java, southeasterly winds generate an Ekman offshore transport of surface water along the coast that induced upwelling (Wyrtki, 1987). Hendiatri *et al.* (2004) found that SeaWiFS chl a higher than 0.8 mg m^{-3} and sea surface temperature (SST) lower than 28°C are indications of upwelling at southern Java. The development of upwelling events varies depending on the strengths of the monsoon (Hendiatri *et al.*, 2004). They further noticed that during November 1997, a very strong upwelling event covered a large area from south Java to the equator around mid of west Sumatra. Murtugudde *et al.* (1999) have highlighted the similar upwelling through anomalous phytoplankton bloom using the SeaWiFS images. In November 1999, the SeaWiFS images showed that no upwelling existed in the same area (Hendiatri *et al.*, 2004). Both Hendiatri *et al.* (2004) and Asanuma *et al.* (2003) have attributed this chl a variation to the El Niño event in the Pacific Ocean.

1.4 Objectives of the study

There were limited oceanography study at the area around MS, Andaman Sea and eastern of BOB. The oceanographic conditions in these areas are rather unknown as there were very limited oceanography studies. Due to the fact that the Malacca Straits has been the most strategic shipping route in the world and the destructive 2004 tsunami that occurred in this areas, we are interested to know how the ocean conditions at these areas has been change for the past few years and the effects of the tsunami on the marine environment by using the ocean color remote sensing technology. The study has been divided into three major sections. The first section will be focused on the seasonal chl a variation in the Malacca Straits and the major force of the variation. The second section will discussed on the interannual variation of the chl a at eastern Indian Ocean, including the Andaman Sea, MS and southeastern BOB. Factors that contribute to the interannual variability were also examined. The third section was mean to assess the possible tsunami effects on the oceanographic conditions at eastern Indian Ocean using MODIS Aqua satellite.

Chapter 2. Seasonal Variability of SeaWiFS Chlorophyll *a* in the Malacca Straits in Relation to Asian Monsoon

2.1 Introduction

Seasonal to interannual changes in phytoplankton biomass and productivity are very important components of the total variability associated with ocean biological and biogeochemical processes (Yoder and Kennelly, 2003). Primary production in the Southeast Asian regions, for instance South China Sea and Indian Ocean, depicts seasonal variability, due to influence of the Asian monsoon. Dey and Singh (2003) found that chl a concentration in southern Bay of Bengal is higher during the NEM compared to the inter-monsoon period. In the areas of South China Sea, phytoplankton was found bloom at Vietnam coast during SWM, and bloom near Luzon Straits during NEM (Tang *et al.*, 1998; Tang *et al.*, 1999; Liu *et al.*, 2002; Tang *et al.*, 2004). In southeastern Java, increase of chl a concentration is found due to upwelling event during SWM (Hendiarti *et al.*, 2004).

Malacca Straits is one of the world's busiest sea-lanes that connects the Indian Ocean to the South China Sea and Pacific Ocean. Chua *et al.* (2000) reveal that the primary productivity in MS is constant throughout the year. Higher phytoplankton is found in the south where water is shallower, and where there is both vertical mixing and high nutrient input from rivers in Sumatra. The average surface chl a is 0.54 mg m^{-3} at northern MS without any distinct seasonal variation (Setiapermana *et al.*, 1984). However, previous investigation of the phytoplankton variability in MS was based solely on data collected from oceanographical

cruises, which provided rather non-synoptic and coarse resolution sampling of overall spatial and temporal pattern. Consequently, the seasonal phytoplankton variability could be poorly quantified.

We hypothesize that chl a in MS experienced seasonal variability which influenced by the monsoon similar to other Asian monsoon regions. By using the satellite ocean color time series data, we were able to investigate the phytoplankton variability in a more synoptic and systematical way. This paper provides evidences of seasonal chl a variation in MS by using the SeaWiFS ocean color images. Factors that contributed to the chl a seasonal variability were also examined.

2.2 Materials and Methods

This study was focused on the MS areas as shown in Fig. 2.1. The partition line of northern and southern MS was located slightly to the north of One Fathom Bank that close to the isobath of 50 m (Dotted line in Fig. 2.1). Daily SeaWiFS level 2 and monthly level 3 ocean color images (version 4) were downloaded from NASA GES Distributed Active Archive Center (DAAC). These ocean color images were further processed and analyzed by using SeaWiFS Data Analysis System (SeaDAS).

NCEP Reanalysis monthly mean wind speed (WS) and topography data were acquired from Live Access Server at the National Virtual Ocean Data System (NVODS) (data available at http://ferret.pmel.noaa.gov/NVODS/servlets/dataset), while monthly wind stress and curl

(WC) data were downloaded from the Fleet Numerical Meteorology and Oceanography Center (FNMOC) datasets at Pacific Fisheries Environmental Laboratory (PFEL) Live Access Server (data available at http://las.pfeg.noaa.gov/las/). Rainfall data from January 1991 to December 2001 was acquired from Malaysian Meteorological Service.

Oceanographic data were provided by the Southeast Asian Fisheries Development Center (SEAFDEC) and Malacca Straits Research and Development Centre (MASDEC). From SEAFDEC oceanographic cruise No. 68, we selected only the data collected during 8 – 9 February 2003 that located within Andaman Sea and Malacca Straits for this analysis. MASDEC had conducted five cruises along Malaysian waters in MS during monsoon and inter-monsoon seasons for the period from 1998 to 2002. The MASDEC oceanographic data used in this study consisted of cruise 1 (23 November - 2 December 1998) (NEM), cruise 4 (29 July - 7 August 2000) (SWM) and cruise 5 (18 - 29 October 2002) (Inter-monsoon). In situ surface chl a from MASDEC cruises were input into ArcView 8.1 GIS for spatial analysis. Daily SeaWiFS level 2 images during each cruise were composite into single image using SeaDAS in order to reduce the effect of cloud cover. Chl a and normalized water leaving radiance at 555 nm (nLw 555) values from these composite images were extracted for the comparison with in situ data.

2.3 Results

2.3.1 Seasonal SeaWiFS chlorophyll a variation

Analysis of the five-year composite monthly mean chl a images showed that there was a seasonal variability of chl a in MS. In the northern part of MS, surface chl a increased from November to March (Fig. 2.2). The high chl a area emanated from the area around Penang to Langkawi Island in November, and extended to the west and northwest in January when the northeast monsoon was fully developed. The high chl a area started decaying since March. During the SWM, chl a in northern MS remained low throughout the season. The chl a increased as much as twice during the NEM compared to SWM. Monthly mean chl a at northern MS (Fig. 2.3A) showed highest concentration during January (1.38 mg m^{-3}) and lowest during August (0.57 mg m^{-3}). The peak of chl a was observed during NEM.

At the coastal and southern MS, SeaWiFS chl a showed more than 2.0 mg m^{-3} throughout the year (Fig. 2.2). Higher chl a was found at the southeastern entrance of MS from June to September during the SWM. Besides, very high chl a was observed at the middle of the Straits at Sumatra Island from November to December. Monthly mean chl a at southern MS (Fig. 2.3A) recorded highest concentration during November (5.39 mg m^{-3}) and lowest during March (3.70 mg m^{-3}). The peak of chl a in southern MS occurred earlier than in northern MS. Maximum chl a at southern MS was about 4 times higher than northern MS. However, the accuracy of SeaWiFS chl a estimation at these shallower areas need to be further examined due to turbid water.

2.3.2 Comparison of MASDEC in situ and SeaWiFS satellite data

During MASDEC cruise 1 (NEM), most of the stations, which located closed to the coastal area showed chl a more than 1.00 mg m^{-3} (Fig. 2.4A). Surface chl a was higher at northern MS than southern MS. Mean surface chl a during cruise 1 was 1.23 mg m^{-3}. Maximum chl a of 2.81 mg m^{-3} was sampled at station 2, whereas minimum chl a was 0.22 mg m^{-3} at station 3 (Fig. 2.4A). During cruise 4 (SWM), higher surface chl a was observed at the middle of the Straits (Fig. 2.4B). Mean surface chl a during cruise 4 was 0.72 mg m^{-3}. Maximum chl a of 3.06 mg m^{-3} was sampled at station 18, whereas minimum chl a was 0.16 mg m^{-3} at station 9 and 13 (Fig. 2.4B). During cruise 4, surface chl a at northern and southern MS was much lower than cruise 1.

Increasing SeaWiFS chl a trend towards southern MS was observed in both cruise 1 and cruise 4 (Fig. 2.5). However, no increasing tendency was observed in MASDEC in situ chl a toward the south. The in situ chl a value was higher for certain coastal stations, for instance station 14 and 18. During cruise 1 (NEW), a few stations at the northern MS showed close values with the in situ chl a. Station 2, 9, 10 and 13 at the north was under-estimated by the SeaWiFS chl a, whereas most of the station at the middle of the Straits showed over-estimation of SeaWiFS chl a (Fig. 2.5A). During cruise 4 (SWM), good correlation between the MASDEC and SeaWiFS chl a was also found at the northern MS (from station 1 to 13, station 15, 16 and 17) (Fig. 2.5B). Whereas, stations to the southern MS and station 14, showed over-estimation of the surface chl a values.

The increasing trend of nLw 555 values for both cruise 1 and 4 was very similar to the SeaWiFS chl a (Fig. 2.5). The analysis results showed that SeaWiFS chl a tended to be over-estimated at the stations with high nLw 555. This observation was evident in cruise 4, where all the over-estimated stations were accompanied with nLw 555 values more than 1.00 mW cm^{-2} μm^{-1} sr^{-1}. During cruise 4, SeaWiFS chl a value at station 14 was over-estimated almost 6 times from the in situ chl a, where the nLw 555 values 5.25 mW cm^{-2} μm^{-1} sr^{-1} was the highest during these two cruises.

Monthly nLw 555 distributions in MS did not show much variation like the chl a distribution. The distribution pattern is always similar, where extremely high value (nLw 555 more than 1.00 mW cm^{-2} μm^{-1} sr^{-1}) at the coastal and southern of MS, while the offshore areas at northern MS were less than 0.50 mW cm^{-2} μm^{-1} sr^{-1} (Fig. 2.6B). Correlation analysis between total suspended sediment (SS) and SeaWiFS showed that the concentration of in situ SS is positively related to the nLw 555 values with $R^2 = 0.71$ (Fig. 2.7). Most of the high SS concentrations were recorded at the southern and coastal stations, which was very similar to the nLw 555 distribution pattern from SeaWiFS satellite.

2.3.3 Monthly wind and rainfall variation

Wind speed at the northern MS showed two peaks during monsoon seasons (Fig. 2.3B). Maximum WS 3.86 m s^{-1} was observed in January during NEM. Besides, another peak of WS 3.43 m s^{-1} was noted in July during SWM. It was generally lower during

inter-monsoon (less than 3.00 m s^{-1}). Wind speed in the southern MS was about half of that in northern MS (Fig. 2.3B). There were two WS peaks at southern MS in July and December. Maximum WS 1.74 m s^{-1} was observed in December, whereas lowest WS 1.25 m s^{-1} in September. At northern MS, the peak of WS in NEM was coincided with the chl a peak; however, chl a did not increased during the peak of WS in SWM. The WS at southern MS was different from the chl a variation.

Wind pattern in MS (Fig. 2.8) showed similar observation as the monthly WS variation mentioned above, where higher WS at the northern part and lower WS in the south. During NEM, higher WS was observed at the areas above latitude 6°N in the Straits (Fig. 2.8A). Strong NEM wind at the South China Sea and Gulf of Thailand was getting weaker when blow across Malay Peninsular. Strong positive WC (more than 0.10 x 10^{-6} Pa m^{-1}) occurred at latitude from 4.5°N to 6.5°N at northern MS. Whereas negative WC -0.10 x 10^{-6} Pa m^{-1} was observed at southern Phuket (Fig. 2.8A). Positive WC is associated with upwelling, while negative WC is associated with downwelling. During SWM, stronger monsoon wind was noted at the northern opening to Andaman Sea (Fig. 2.8B). Most of the area at northern MS showed negative WC, particularly very strong negative WC (lower than -0.20 x 10^{-6} Pa m^{-1}) was observed at the northern Sumatra. Briefly, the WC pattern at northern MS was very much differing between the two monsoons.

Monthly rainfall variation at Malay Peninsular illustrated some similarities (Fig. 2.3D). Both rainfall stations at Langkawi and Malacca showed increasing trend from NEM, and

reached the peak during inter-monsoon or early NEM, and lowest rainfall during NEM. Rainfall at Langkawi showed more variation than Malacca. At Langkawi, highest monthly mean rainfall 389 mm was recorded in October, and lowest 24.6 mm in Janaury. The trend of monthly rainfall at Langkawi was much different from both chl a and WS monthly variation. At Malacca, maximum rainfall 247 mm was recorded in November, and minimum rainfall 86.8 mm in February. The increasing trend of rainfall at Malacca was similar to the increasing trend of SeaWiFS chl a at southern MS. Besides, the peak of rainfall at Malacca was coincided with the SeaWiFS chl a peak at southern MS.

2.4 Discussions

2.4.1 Discrepancy of SeaWiFS chlorophyll a estimation

The coastal water in Malacca Straits is very turbid due to the rivers discharge and the resuspension of bottom sediment from tidal (Chua *et al.*, 1997). In areas around the river mouth and the coastal region, water transparency is less than 10.0 m (Chua *et al.*, 1997). SeaWiFS chl a OC4 algorithm is known to be broken down in area loaded with high SS or CDOM (IOCCG, 2000). Studies in Korean waters by Ahn *et al.* (2001) found that the presence of SS in coastal areas lead to overestimation of chl a concentration greater than 20 – 500%.

The 555 nm band on SeaWiFS sensor is found to be particularly good at detecting the reflectance of light from suspended sediment (Acker, 2005). Our study showed that the nLw

555 values were closely related to the SS in MS. As the result, the over-estimation of SeaWiFS chl a at coastal and southern water in MS could be due to the high SS. After rainfall, more sediment will be flushed into the sea, thus, the effect of SS on the chl a estimation is expected to be more severe during rainy season. Consequently, higher chl a at southern MS during rainy season was likely been over-estimated. Beside the high SS, CDOM could be another factor that contributed to the inaccuracy of chl a estimation. There are many rivers and mangrove forests along the coastal areas, especially at the southern MS. The effect of CDOM could be the significant for the coastal water that close to these CDOM sources. There was some under-estimation of chl a from SeaWiFS when compared to the MASDEC in situ data. We suspected that this discrepancy was caused by the temporal differences between the sampling day and the satellite data that available.

In contrast to the southern MS, the comparatively high SeaWiFS chl a in the northern MS during NEM is likely not as artifact but a phytoplankton bloom. Monthly SeaWiFS chl a image on January 2002 showed high chl a area extended from the Penang to Langkawi coast toward northern Sumatra Island (Fig. 2.6A). However, nLw 555 values in the tongue of high chl a area in northern MS was lower than in coastal area (nLw 555 less than 0.60 mW cm^{-2} μm^{-1} sr^{-1}) (Fig. 2.6B). Slight increased of the nLw 555 nm in this area could probably attributed to the increased of turbidity by phytoplankton cells. The MASDEC cruise 1 (NEM) in situ chl a at northern MS appeared to be higher than cruise 4 (SWM) (Fig. 2.4).

Northern MS was experiencing the dry season during NEM (Fig. 2.3D). Low rainfall

is expected to reduce the chl a as there is less nutrient input from the river. Besides, less sediment and CDOM will be discharged into the sea. Hereby, we further conceived that the increase of chl a at northern MS was contributed by the blooming of phytoplankton and the effects of SS and CDOM were negligible. There was other mechanism, except the river discharge, that helped supplying the nutrient for the phytoplankton bloom during NEM.

2.4.2 Ekman Pumping

The offshore surface water of northern MS is basically oligotrophy (Yusoff *et al.*, 2001). Hence, any physical mechanism that is capable to supply nutrient to the surface water would be important for the NEM bloom. When the NEM wind started blowing across the northern MS from the northeast direction, the surface water seem to be advected offshore toward the Andaman Sea. Wind pattern analysis showed that the northwest open area in MS (latitude more than 5.5°N) received stronger influence of the monsoon wind than other areas inside the Straits (Fig. 2.8A). Monsoon wind is relatively weak in the southeastern part of the study area due to the topological influence of the high mountain range in both Malay Peninsular and Sumatra (Namba and Ibrahim, 2002). Positive WC at latitude from 4.5°N to 6.5°N was attributed to the wind pattern in that area (Fig. 2.8A).

Consequently, the positive WC had induced positive EP rate that caused upwelling at northern MS (Fig. 2.3C). Corroborating evidence of upwelling event was observed during SEAFDEC cruise No. 68 which included measurements at a number of stations in MS (see Fig.

2.1). High saline water (33.5 p.s.u.) was upwelled from 50 m at station 58 until 25 m at station 59 (Fig. 2.9). It is expected that upwelling had brought nutrient from the deep water to the surface water that initiating the phytoplankton bloom. This upwelling event was apparently distinct from the previous findings near One Fathom Bank located in the middle part of MS (Wyrtki, 1961; Uktolseya, 1988; Chua *et al.*, 1997). The effect of river discharge was observed at station 62 and 63 (Fig. 2.9), where the surface salinity was much lower compared to the stations at north.

The EP analysis results suggested that the upwelling phenomena were confined only to the narrow positive wind curl area in northern MS. At point A (Fig. 2.1), maximum EP rate was 3.53 m day^{-1} in December (Fig. 2.3C). However, point B, which is located outside of the positive wind curl areas, did not show significant pumping rate during NEM. The intensification of EP during NEM agreed well with the development of the chl a bloom (more than 1 mg m^{-3}) that started in the east of northern MS at latitude from 4.5°N to 6.5°N (from Penang to Langkawi Island) and extended toward Andaman Sea (Fig. 2.2). The possible mechanism of the NEM bloom in northern MS can be explained as follows:

At the beginning of the bloom (November), chl a increased along the coastal areas. When the NEM fully developed in December, strong upwelling by EP occurred along 4.5°N to 6.5°N in the Straits. This upwelling phenomenon was important in supplying nutrients to phytoplankton for maintaining its bloom throughout the northern MS, and along to the continental slope at northern Sumatra from January to March. When the NEM wind was

weakening during inter-monsoon, the bloom was simultaneously reduced.

During SWM, when the strong southwesterlies reached eastern Indian Ocean, the high mountain ranges in Sumatra block the strong wind from MS. As the result, the WS in MS was much lower as compare to the open ocean near Andaman Sea (Fig. 2.8B). Strong negative WC occurred due to the large differences of WS at northern tip of Sumatra (Fig. 2.8B). The negative WC caused negative EP rate (Fig. 2.3C) and induced downwelling event in the study area between May and September. As there was no further supply of nutrient to the surface water, the chl a concentration remained low throughout SWM.

2.4.3 Comparison to other regions

The seasonal chl a variation in MS suggests that it is similar to other Asian Monsoon regions, where the chl a variation is in relation to the monsoon wind. Most of these areas show the chl a peak during monsoon either in NEM or SWM. Tang *et al.*, (2004) reported that the phytoplankton bloom at eastern Vietnam from June and decay in October. The chl a reaches a peak of 0.9 mg m^{-3} in August during SWM (Liu *et al.*, 2002). In northwestern of Luzon, the bloom starts in October, and reveals a strong peak (0.5 mg m^{-3}) in December (Liu *et al.*, 2002). The Luzon phytoplankton bloom started much earlier compared to the phytoplankton bloom at northern MS could probably attribute to the higher latitude of Luzon, where the influence of NEM begins earlier.

Monsoon induces upwelling event is one of the major factor that contributed to the

phytoplankton bloom in Southeast Asian monsoon regions. Although the main force of the upwelling was the monsoon wind, the mechanism of upwelling could be different due to different local conditions. In southern Java, the coastal upwelling is caused by the southeasterly alongshore winds that generate an Ekman offshore transport of coastal water (Susanto *et al.*, 2001). In the coast of Vietnam, Xie *et al.* (2003) revealed that in addition to the classical coastal upwelling mechanism, EP associates with a wind jet offshore is important for the ocean upwelling off the coast. A strong wind jet occurs when the southwesterly wind impinge on Annam Cordillera (mountain range on the east coast of Indochina) resulting in positive WC and intense open ocean EP (upwelling) (Xie *et al.*, 2003). The mechanism of the EP induced upwelling off Vietnam was very similar to northern MS. However, compared to the single mountain range in Vietnam coast, both the mountain ranges in Peninsular Malaysia and Sumatra Island act as the double shield of monsoon wind on the left and right of MS. This unique topography in MS has produced both upwelling and downwelling events over the same area in northern MS during different monsoon. These monsoon induced upwelling are important phenomena that support and enrich the local fishery resources of the region.

2.5 Conclusion

Seasonal SeaWiFS chl a variation in MS is different between the northern and southern areas. This study demonstrates that the seasonal phytoplankton variability in northern MS is strongly influenced by the Asian monsoon wind and the land topography. The

coastal and southern waters in MS having complex optical properties that could mislead the standard chl a estimation. Development of local algorithm will help to increase the accuracy of the chl a prediction. This is the first study that found phytoplankton bloom at northern MS during NEM. The discovery of phytoplankton bloom at northern MS has altered our understanding of the spatial and temporal extent of the primary productivity in MS, which has been previously considered seasonally invariant. The surface enrichment and phytoplankton bloom throughout northern MS could play an important role in sustaining the rich fishery resources in this area. Understanding these mechanisms will aid to forecast the possible biological response and could further assist in the marine resource management practices.

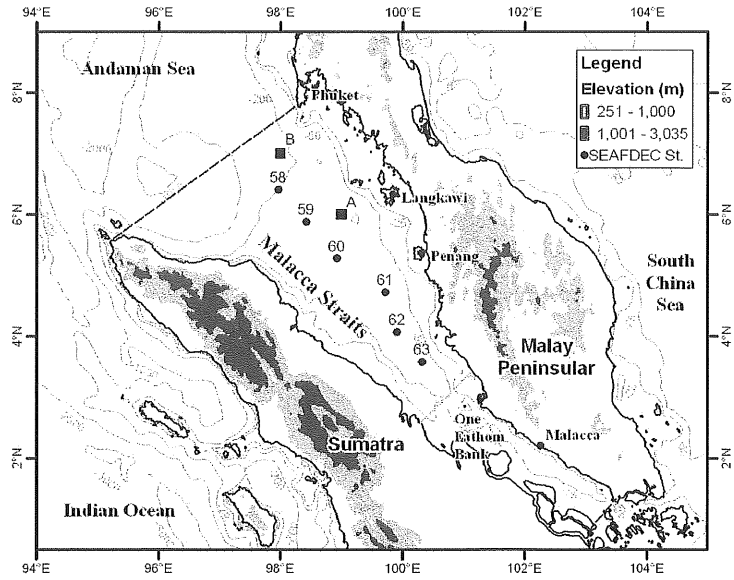

Fig. 2.1 Bathymetry and topology of Malacca Straits and its surrounding areas. Shaded areas on land show the mountain ranges in both Sumatra and Malay Peninsular. SEAFDEC cruise No. 68 stations 58-63 are marked. Dark dotted lines show the boundary of Malacca Straits. Gray dotted line at the middle of the Straits shows the division of the northern and southern areas.

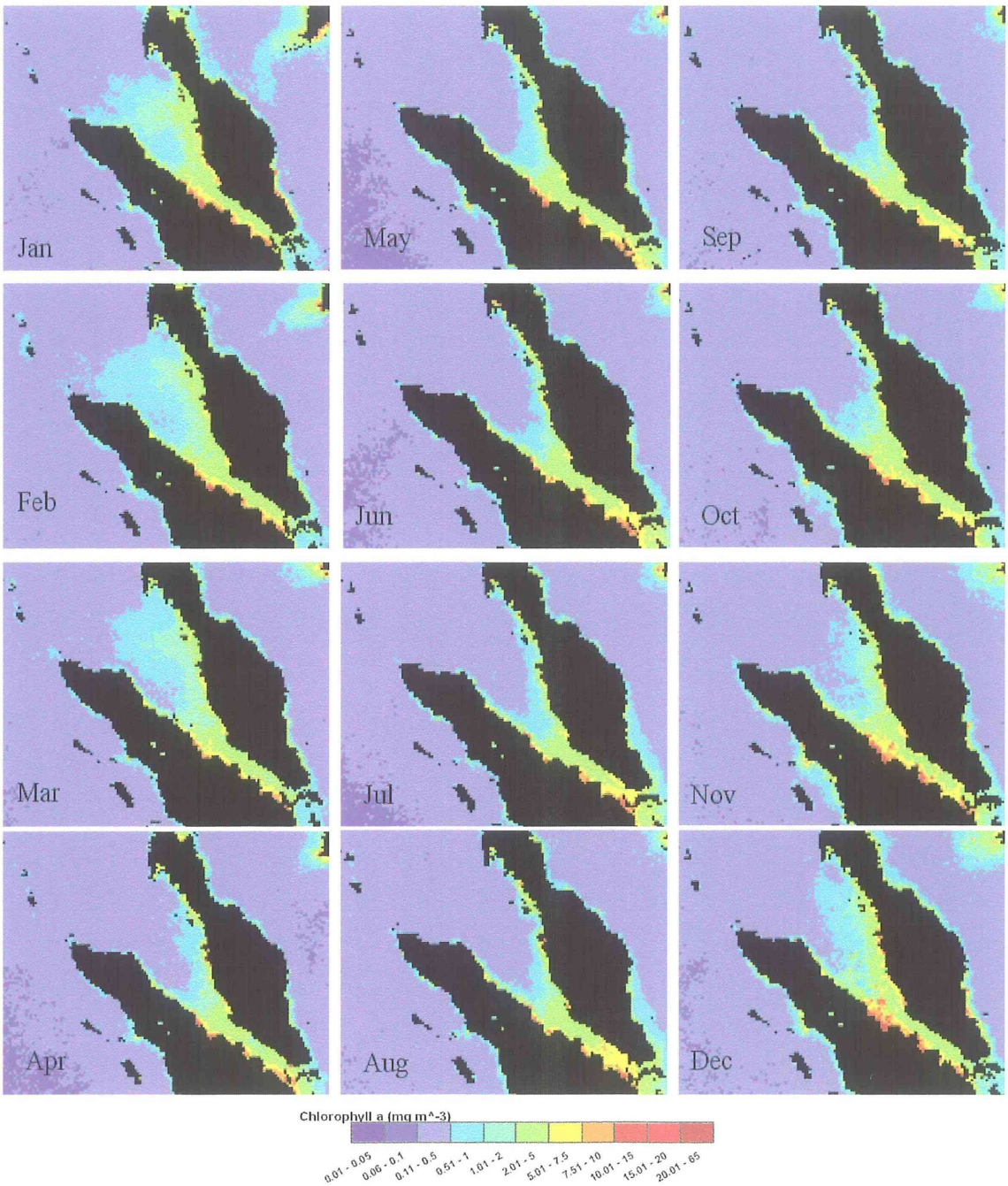

Fig. 2.2 Monthly composite of SeaWiFS chlorophyll a (mg m^{-3}), 1998 - 2002.

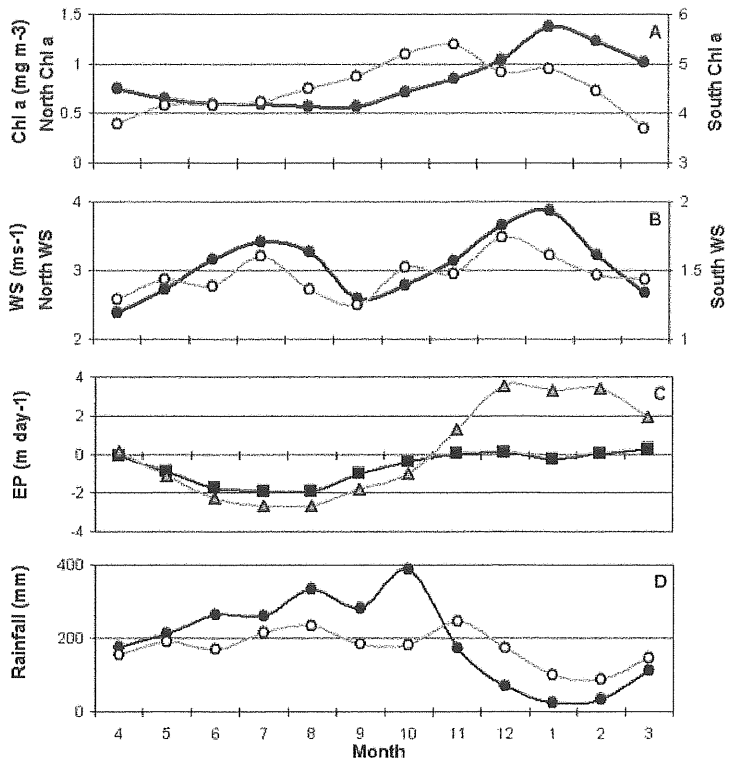

Fig. 2.3 Monthly mean SeaWiFS chlorophyll a (chl a) (mg m^{-3}) (A) and NCEP reanalysis monthly mean wind speed (m s^{-1}) (B) averaged over northern (●) and southern (○) MS. The scale for northern and southern MS is located on the left and right, respectively. Monthly Ekman pumping rate (m day^{-1}) (C) is calculated using the FNMOC wind stress curl data for two locations at 6°N 99°E (Point A, Δ) and 7°N 98°E (Point B, ■) as shown in fig. 2.1. Monthly rainfall (mm) (D) at Langkawi (●) and Malacca (○) (Locations shown in fig. 2.1) averaged over the period from 1991 until 2001.

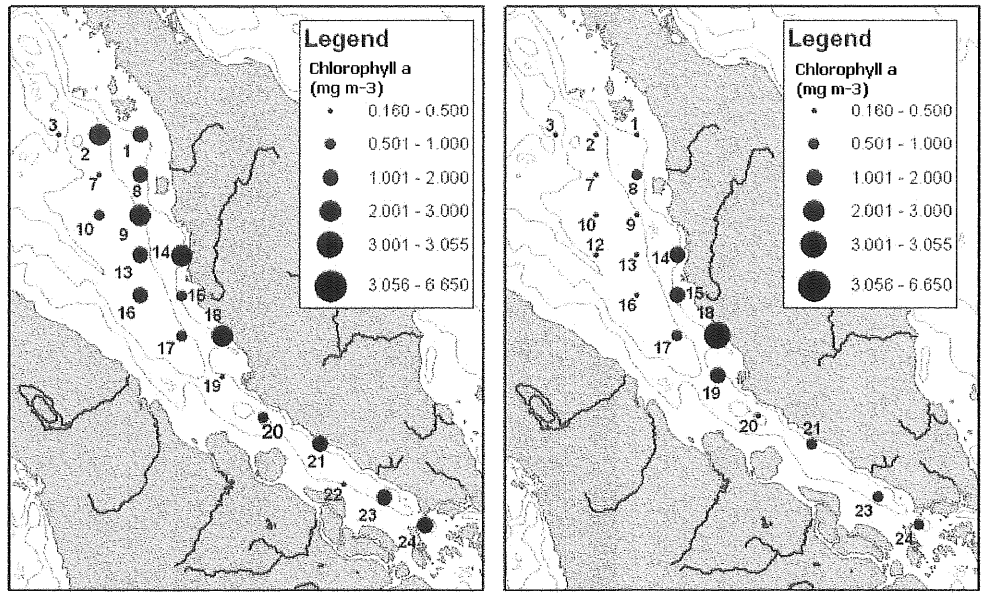

Fig. 2.4 In situ chlorophyll a (mg m^{-3}) of MASDEC oceanographic cruises. Cruise 1 (A) was conducted during NEM (23 November – 2 December 1998) and cruise 4 (B) was conducted during SWM (29 July – 7 August 2000).

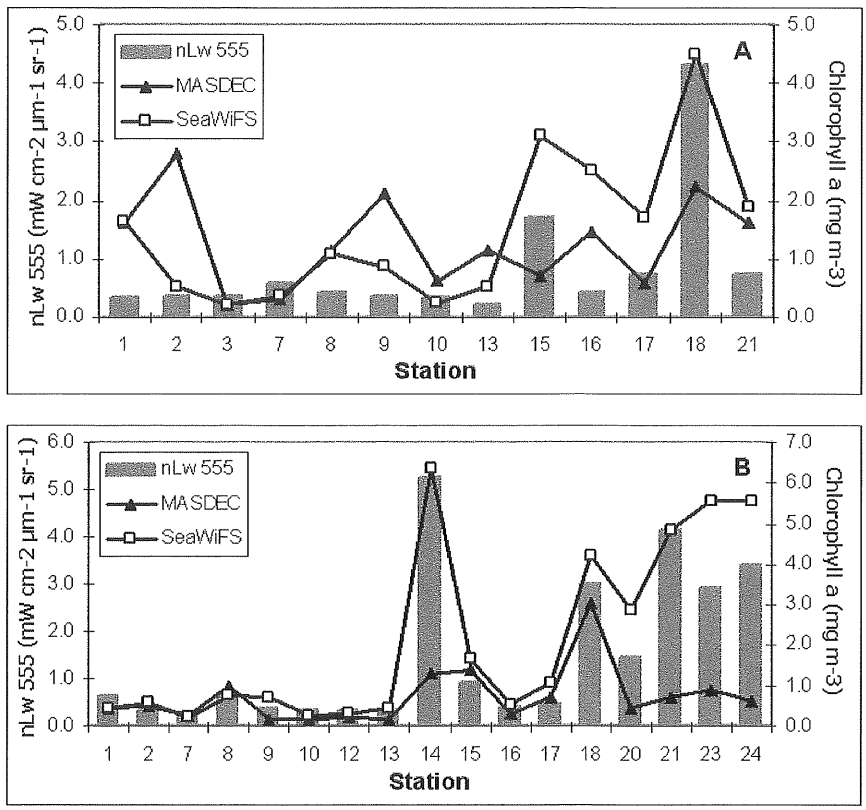

Fig. 2.5 MASDEC in situ chlorophyll a (mg m^{-3}) (▲), composite SeaWiFS chl a (mg m^{-3}) (□), and composite normalized water leaving radiance at 555 nm (mW cm^{-2} μm^{-1} sr^{-1}) (bar) during MASDEC oceanographic cruise 1 (A) and cruise 4 (B).

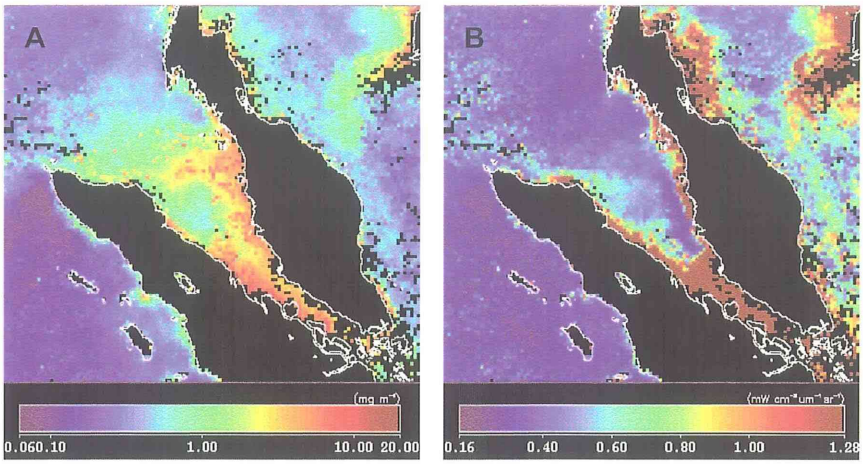

Fig. 2.6 Monthly SeaWiFS chlorophyll a (mg m^{-3}) (A) and normalized water leaving radiance at 555 nm (mW cm^{-2} μm^{-1} sr^{-1}) (B) image on January 2002. Cloud cover and noise is colored black.

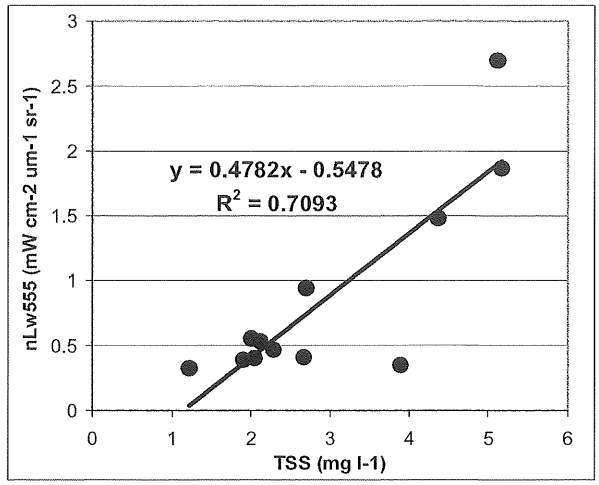

Fig. 2.7 Correlation of MASDEC in situ total suspended sediment (mg l^{-1}) (TSS) and composite SeaWiFS nLw 555 values (mW cm^{-2} μm^{-1} sr^{-1}) (nLw 555) of MASDEC oceanographic cruise 5 (18-29 October 2002).

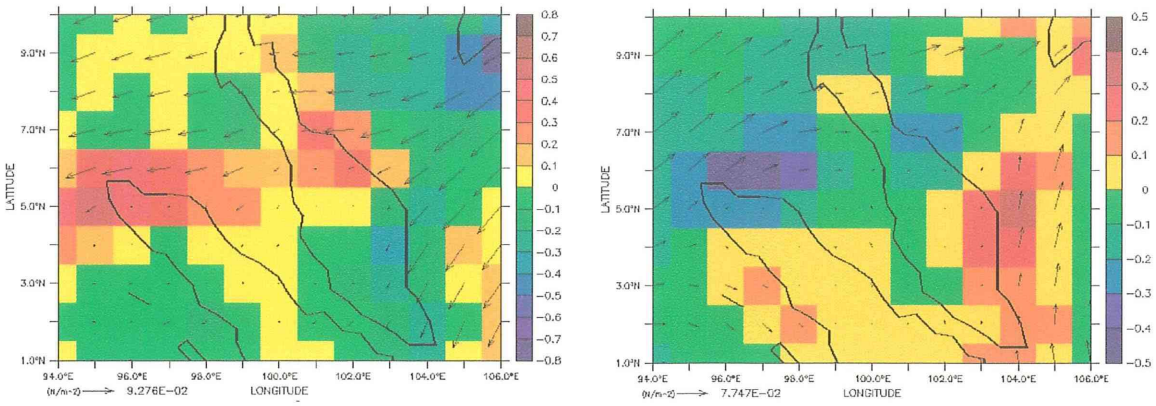

Fig. 2.8 FNMOC surface wind stress (N m^{-2}) and curl (Pa m^{-1} x 10^{-6}) during January 2002 (A) and July 2002 (B). The wind stress (vector) is superimposed on the curl of wind stress (raster).

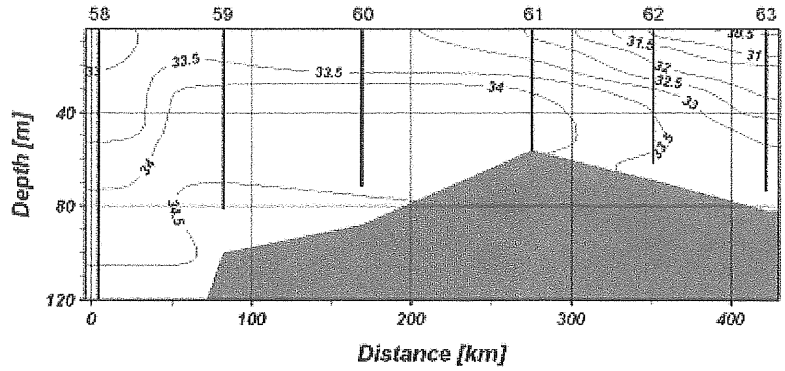

Fig. 2.9 Bathymetry and vertical salinity profiles (psu) for the SEAFDEC Cruise No. 68 (8-9 Feb 2003) showing the transect from northwest to southeast along northern MS. Locations of the sampling stations (58-63) are shown: see also Fig. 2.1. Gray color shows sea floor.

Chapter 3. Interannual Chlorophyll a Variation at the Southeastern Bay of Bengal during Northeast Monsoon

3.1 Introduction

The SeaWiFS ocean color sensor has provided the first successful observations of the evolution of biological response in the Pacific Ocean during the biggest El Niño-Southern Oscillation event (ENSO). In the Indian Ocean, it also observed an anomalous phytoplankton bloom during October-December 1997 coinciding with the anomalous upwelling and cooling in the eastern equatorial region and off the coast of Sumatra (Murtugudde *et al.*, 1999; Hendiarti *et al.*, 2004). Saji *et al.* (1999) and Webster *et al.* (1999) reveal that this cooling event is unique and inherent in the Indian Ocean, and it is known as the Indian Ocean Dipole (IOD). Saji *et al.* (1999) constructed a of dipole mode index (DMI) using the SST anomaly across eastern and western Indian Ocean basin to identify the dipole mode event, which resemble the Southern Oscillation Index (SOI) that help to identify the ENSO event in Pacific Ocean.

Many studies utilizing ocean color remote sensing at BOB focused on the chl a variations around the western boundary of the Bay (Gomes *et al.*, 2000; Prasanna Kumar *et al.*, 2002; Dey and Singh, 2003; Vinayachandran and Mathew, 2003) and Sri Lanka (Kasyapa, 2000; Vinayachandran *et al.*, 2004). Dey and Singh (2003) found higher chl a concentration at southern BOB during the NEM compared to those during pre- and post-monsoon period. The NEM wind that induces the open ocean upwelling driven by EP is considered to be the major

factor for the intensification of chl a bloom in BOB (Vinayachandran and Mathew, 2003). In the northeastern MS, the seasonal occurrence of phytoplankton bloom has been attributed to the NEM wind-driven EP (Tan *et al.*, 2006). A high chl a tongue that emanates from the eastern Malacca Straits is extended into the Indian Ocean through northern Sumatra (Tan *et al.*, 2006).

Little is known about the oceanography of Southeastern Bay of Bengal (SEBOB) until after the 26 December 2004 South Asian tsunami. Researchers focused on the effects of the destructive waves in these areas, but due to insufficient historical and in-situ data, the assessment of the tsunami effect will be difficult. In an attempt to understand the interannual chl a variation of SEBOB, we analyzed the time-series SeaWiFS ocean color data during NEM. The factors that could possibly contribute to the interannual chl a variability were examined. The anomalous phytoplankton bloom during NEM 1997 – 98 was further investigated. To the end, the effects of the large-scale atmospheric-ocean dynamics on interannual chl a variation were discussed.

3.2 Materials and Methods

The study area covers the SEBOB, MS and southern Andaman Sea (Fig. 3.1), with upper left limit at 11.0°N 88.0°E, and lower right limit at 1.0°N 102.0°E. Monthly SeaWiFS level 3 ocean color images (version 4) for the period from October 1997 – December 2004 were downloaded from NASA GES DAAC. These ocean color images were further processed

and analyzed using SeaDAS.

To understand the role of atmospheric forcing on ocean, monthly data on WS and WC were downloaded from the FNMOC datasets at PFEL Live Access Server (data available at http://las.pfeg.noaa.gov/las/). To infer the surface signature of the ocean, Archiving, Validation and Interpretation of Satellite Oceanographic data (AVISO) sea surface height anomaly (SSH) data were acquired from AVISO Live Access Server (data available at http://las.aviso.oceanobs.com/las/servlets/dataset), while TOPEX/Poseidon SSH anomaly were downloaded from the NASA JPL POET PO.DAAC OceanESIP Tool website (data available at http://poet.jpl.nasa.gov/).

The DMI was acquired from Indian Ocean Dipole Homepage provided by Frontier Research System for Global Change (FRSGC) (data available at http://www.jamstec.go.jp/frcgc/research/d1/iod/), whereas SOI was acquired from NOAA - CIRES Climate Diagnostics Center (data available at http://www.cdc.noaa.gov/Correlation/soi.data). To access the role of stratification, oceanographic data were provided by the SEAFDEC. Besides, Array for Real-time Geostrophic Oceanography (ARGO) Float data were downloaded from US Global Ocean Data Assimilation Experiment (GODAE) ARGO GDAC Data Browser (data available at http://www.usgodae.org/cgi-bin/argo_select.pl). The ARGO data are import into Ocean Data View (ODV) software for analysis (software available at http://odv.awi-bremerhaven.de/).

3.3 Results

3.3.1 Monthly chlorophyll a variation

Monthly chl a at SEBOB exhibited seasonal variation (Fig. 3.2). Higher chl a was observed during NEM than SWM. Maximum chl a (0.32 mg m^{-3}) occurred during January, while minimum chl a (0.20 mg m^{-3}) during June. Higher deviation of chl a was observed during NEM from December to March, whereas the chl a during SWM (June – August) did not show much deviation. As the chl a at SEBOB was higher and exhibited more variability during NEM, our study was focused on the NEM period.

3.3.2 Interannual chlorophyll a variation

Surface chl a at SEBOB showed clear interannual variation during January (Fig. 3.3). Two areas that exhibited large variation were the northeastern MS and the western Nicobar Island until northwestern Sumatra (here after NWS). In January 1998, large phytoplankton bloom occurred at eastern Indian Ocean, specifically along the western coast of Sumatra and NWS. This period was associated with the IOD event. The monthly chl a variation during IOD 1997 - 98 will be discussed in detail in section 3.3.4. In January 1999 and 2001, surface chl a was very low along the eastern Indian Ocean. Slight increased in chl a at SEBOB occurred during January 2002 and 2004. A patch of chl a around 1.0 mg m^{-3} extended to 90.0°E in January 2002 and 2004.

The chl a at northeastern MS was much higher than in NWS (Fig. 3.3). High chl a

tongue (about 5.0 mg m^{-3}) was observed stretching towards the northern Sumatra in January 2000, 2002 and 2004. However, during January 1998, the high chl a tongue did not intensify even though the chl a at eastern Indian Ocean was anomalously high. The chl a at western and center of Andaman Sea was always low (less than 0.5 mg m^{-3}). The increase of chl a at southern Andaman Sea exhibited close relationship with the chl a tongue in MS.

3.3.3 Relationship of chlorophyll a, wind speed and sea surface height

To investigate the factors that influence interannual chl a variability at SEBOB, we compared the chl a variation with WS and SSH during NEM for both NWS (92.0°E) and MS (98.0°E) along 6.0°N. Results showed that chl a profile at 92.0°E and 98.0°E exhibited distinct interannual variation (Fig. 3.4A), although both WS and SSH patterns at these two locations were quite similar (Figs. 3.4B and 3.4C). Highest chl a anomaly at 92.0°E was recorded during January 1998 (Fig. 3.4A). Positives anomaly was also observed during NEM 1999 - 2000, 2001 – 02 and 2003 – 04. However, during NEM 1998 - 99, 2000 – 01 and 2002 – 03, chl a showed negative anomalies. The peak of chl a at 92.0°E coincided with the lowest SSH (Fig. 3.4C) that occurred during NEM.

Mean chl a during NEM at 92.0°E and 98.0°E were 0.23 mg m^{-3} and 0.67 mg m^{-3}, respectively (not shown). Chl a at 98.0°E was three times higher than that at 92.0°E. The chl a at 98.0°E exhibited an increasing trend from November 1997 to February 2004 (Fig. 3.4A). Highest chl a anomaly was recorded in January 2004, whereas lowest chl a was recorded in

November 1998. During periods of large chl a bloom at 98.0°E (NEM 1999 – 00, 2001 – 02 and 2003 – 04), the peaks occurred in January, whereas during periods of smaller chl a bloom (NEM 1998 – 99, 2000 – 01 and 2002 – 03), the peaks occurred in February. The very high chl a peaks observed during January 2000 and 2002 coincided with the high WS peaks (Figs. 3.4A and 3.4B). The chl a peak at 98.0°E in January 2004 did not coincide with the smaller WS peak that occurred one month earlier, but the SSH was decreased during the same period (Fig. 3.4C). The decline in SSH occurred a month earlier (January) in 2004 than the previous years (February 2002 and 2003).

The anomalously low SSH during NEM 1997 - 98 was observed at both 92.0°E and 98.0°E. However, only the chl a anomaly at 92.0°E exhibited large increase. The WS at 98.0°E was rather low in NEM 1997 – 98. By further examining the correlations between the chl a, WS and SSH, we found the chl a at 92.0°E was negatively correlated with the SSH with $R = 0.80$ ($p < 0.001$), whereas the chl a at 98.0°E was positively correlated with WS with $R = 0.65$ ($p < 0.001$) (Fig. 3.5). We found lower correlation between chl a and WS at 92.0°E ($R = 0.33$) and chl a and SSH at 98.0°E ($R = 0.48$) (not shown).

3.3.4 Indian Ocean Dipole 1997 - 98

The IOD 1997 – 98 was coincided with the strong El-Niño event in the Pacific Ocean (see SOI in fig. 3.4D). The IOD event started during summer 1997 and reached its peak during autumn 1997. However, the effects were observed until winter 1997 – 98, where the

DMI exhibited strong positive values (Fig. 3.4D). Wind stress data during October – November 1997 showed the occurrence of anomalous alongshore wind at western Sumatra coast (Fig. 3.6). SSH was low (about –20.0 cm) at eastern Indian Ocean during the same period. Large chl a bloom was observed which extended farther to the west. A chl a patch with concentration of around 1.0 mg m^{-3} spread all the way to Maldives (70.0°E) along the equator. This bloom started decaying in January 1998 when the anomalous southeast wind became weaker.

Another large phytoplankton bloom was observed at NWS, which started much later than the chl a bloom at the equator. Surface chl a at NWS began to increase in November 1997 and reached a peak during February 1998. Meanwhile, positive WC occurred at the northern tip of Sumatra (95.0°E 6.0°N). WC more than 0.1 x 10^{-6} Pa m^{-1} was observed in November 1998, and it persisted until March 1998. The SSH at SEBOB was low during October 1997. A low SSH area at NWS (less than -20.0 cm) intensified in December 1997. The bloom of chl a coincided with the area of low SSH. During January 1998, a high chl a tongue (about 1.0 mg m^{-3}) reached eastern Sri Lanka. This bloom extended towards Maldives in February 1998. The propagation of chl a was very similar to the westward extension pattern of low SSH from NWS. With the disappearance of low SSH (-20.0 cm), the chl a bloom decayed in March 1998.

High positive WC (more than 0.1 x 10^{-6} Pa m^{-1}) occurred in the MS and in the southern NWS areas (Fig. 3.6). The high chl a tongue in MS coincided with the high WC in

the Straits. However, the high chl a bloom at NWS was located to the north of the high WC areas.

3.3.5 Vertical temperature profile during 1997 - 98

To investigate the actual conditions in the ocean during the IOD event in NEM 1997 – 98, we analyzed the SEAFDEC XBT data of SEBOB before and during the IOD event. Result showed that the permanent thermocline was located at around 170 m depth (Fig. 3.7). Before the IOD (20 March 1997), the vertical temperature profile showed higher temperature from surface to 100 m depth compared to that during IOD. The surface temperature was 30.1°C, and the temperature at 100 m was 22.5°C (20 March 1997). Strong stratification was observed in the water column where the surface mixed layer was less than 20 m. During the autumn (22 October 1997), when the IOD reached the peak, the 20°C water shoaled from about 110 m to 60 m, while the 25°C water shoaled from 80 m to 42 m. At the end of the IOD (16 February 1998), the 20°C water was observed at 104 m, which was quite close to the depth before IOD.

3.4 Discussions

Nutrient availability is an important factor that determines the increase of phytoplankton in tropical ocean. In the BOB, the upper 30 m of the water column is depleted of nitrate (Prasanna Kumar *et al.*, 2002). Our analysis found that strong stratification occurred

at the water column before the IOD event in autumn 1997 (Fig. 3.7). This strong surface stratification could inhibit the nutrient supply from below thermocline into the surface water.

Strong stratification of the surface water at the BOB has been previously described by some researchers (Gomes *et al.*, 2000; Rao *et al.*, 2002; Prasanna Kumar *et al.*, 2002; Prasanna Kumar *et al.*, 2004). Monsoonal river input from the Indian and Indochinese subcontinents produces low salinity water mass known as BOB Water (Tomczak and Godfrey, 2002). It spreads across the Bay in a nearly 100 m thick layer, producing a strong halocline underneath, which keeps the surface salinity in the eastern Bay below 33.0 psu throughout the year. Its influence extends well into the southern Bay until almost 1.0°N (Tomczak and Godfrey, 2002).

Prasanna Kumar *et al.* (2002) found that even the monsoon wind is unable to erode the strongly stratified surface layer in the BOB. In order for the phytoplankton to bloom, the strong surface stratification must be reduced and nutrient must be supplied from the subsurface layer. We suspected that other physical processes in SEBOB helped to reduce the stratification, thus enabling the chl a bloom in some years.

3.4.1 Effects of monsoon wind

Although NWS is situated within the proximity of MS and both receive similar atmospheric and oceanic forces, their surface chl a variation exhibited some degree of differences (Fig. 3.4). This variability could be due to the difference in depth at these two

areas. The depth of northeastern MS is about 100 m as compared to more than 2000 m in NWS (Fig. 3.1). Despite the strong surface stratification, the NEM wind was able to enhance the surface nutrient and caused phytoplankton bloom in MS due to the shallower depth.

Tan *et al.* (2006) reveal that the chl a bloom at northeastern MS is due to the positive WC that caused EP, which replenish the nutrient at surface from deep water. The positive WC is caused by the NEM wind blowing through the mountains at the northern Malay Peninsular. Concurrently, the variation of EP rate was directly related to NEM wind. During NEM 1999 – 2000 and 2001 – 02, the higher chl a in MS was attributed to higher EP by strong NEM wind (Figs. 3.4A and 3.4B). The higher EP rate had injected more nutrients from the subsurface water into the euphotic zone for supporting the large phytoplankton bloom. Similar EP driven phytoplankton bloom event is also reported in the Costa Rica dome region, where strong coherence is found between the chl a and the WC (McClain *et al.,* 2002). This Central American region is known for strong coastal upwelling and wind jets blowing pass through Central American Mountain from the Atlantic (McCreary *et al.,* 1989).

Monsoon wind at the SEBOB varies from year to year. The monsoon wind variability is closely related to the large atmospheric-ocean dynamics in both the Indian and Pacific Oceans. During 1998 and 1999, NEM wind was weaker due to weakening monsoon induced by strong El-Niño and the persistent high pressure system in western Pacific (Wang *et al.*, 2002; Xie *et al.*, 2003). Xie *et al.* (2003) show that persistent high pressure strongly modulates the wind jet off Vietnam in South China Sea during summer 1998, thereby

inducing higher SST and reducing plankton activity. In the MS, the lower WS could have caused the negative chl a anomalies during NEM 1998 – 99 (Fig. 3.4A). Furthermore, the increase in SSH after the IOD event was expected to elevate the surface stratification that further suppressed nutrient supply to the surface water. As the nutrient at the surface water was limited, increase of phytoplankton was absent during NEM 1998 – 99.

3.4.2 Effects of IOD

The large chl a bloom during IOD 1997 – 98 at the southern coast of Sumatra and Java was attributed to the anomalous alongshore wind (Fig. 3.6). Many researchers have explained this anomalous upwelling event in detail (Murtugudde *et al.*, 1999; Saji *et al.*, 1999; Webster *et al.*, 1999; Hendiarti *et al.*, 2004). Besides the bloom at southern Sumatra and Jave, another large chl a was observed originated from the NWS (Fig. 3.6). Murtugudde *et al.* (1999) reveal that the chl a bloom at NWS was driven by the local WC anomalies. However, we found that the positive WC occurred at NWS every NEM season, but the chl a bloom was missing in January 1999 and 2001 (Fig. 3.3). In February 1998, the high chl a patch extended from NWS toward southwest, Murtugudde *et al.* (1999) described that this bloom is advected to the west by NEC. In fact, our findings showed that the extension of the high chl a tongue exhibited a similar extension pattern with the anomalous low SSH from NWS towards southern Sri Lanka during NEM 1997 – 98 (Fig. 3.6), and significant negative correlation was found between the chl a and SSH (Fig. 3.5).

We suggested that the chl a bloom from the NWS during NEM 1997 – 98 was mainly attributed to the lowering of SSH, which caused the shoaling of thermocline (Fig. 3.7). The lowering of SSH has also reduced the strong near-surface stratification at the surface water. Positive WC induced divergence within these low SSH areas and nutrient were supplied to the surface water to support the phytoplankton bloom. Strong relationship between chl a and SSH has been observed in various scale from the upwelling areas with shallow thermoclines, to the cyclonic eddies thermocline doming regimes (McGillicuddy *et al.*, 1998; Prasanna Kumar *et al.*, 2004) and propagating Rossby waves (Cipollini *et al.*, 2001; Siegel, 2001; Uz *et al.*, 2001; Wilson and Adamec, 2002). In the eastern Pacific Ocean, the chl a is strongly correlated to SSH during ENSO (Wilson and Adamec, 2002).

During the IOD event in 1997 - 98, upwelling coastal Kelvin wave excited at the eastern boundary propagated northward along the periphery of the Bay of Bengal as one branch and southward along the Sumatra coast as another branch (Rao *et al.*, 2002). Han and Webster (2002) have successfully produced the sea level interannual variability in the BOB using a reduced-gravity model. They found that at the eastern and northern boundaries of BOB, sea level anomalies are predominantly caused by equatorial wind variability, which generates coastal Kelvin waves that propagate into the bay along the eastern boundary. Thus, the interannual variability of SSH at SEBOB was closely related to the IOD event, which further affects the surface chl a variation.

3.4.3 Rossby wave, surface currents and eddies

Han and Webster (2002) found that during February 1998, the negative SSH in the eastern and northern bay strengthens and extends farther along the coast and to the interior of the bay due to coastal Kelvin waves and westward radiated Rossby waves. The propagation of the anomalous low SSH from NWS as observed in our analysis was the Rossby wave, which has been described by Han and Webster (2002).

Chl a was expected to increase and later decay after the passage of the wave. It can be clearly seen during February to March 1998 (Fig. 3.6), where the high chl a caused by the Rossby wave at 72° - 88°N in February 1998 was reduced after the low SSH disappear in March 1998. However, a high concentration of chl a remained at the eastern Bay (88° - 95°N) after the passage of Rossby wave, where it continued to be maintained until April 1998 (Fig. 3.6). We suspected that this observation was associated with the surface currents and eddies in these areas.

During NEM, there are three major currents in SEBOB, namely the North Equatorial Current (NEC), North Equatorial Counter Current (NECC) and Equatorial Current (EC) (Fig. 3.8) (Hacker *et al.*, 1998). The vertical profile of ARGO float No. 200270 during December-January 2004 showed the evidence of the high saline water intrusion from Arabian Sea to the eastern BOB (Fig. 3.9). The sampling location of this ARGO float was very close to the theoretical location of the NEC (Fig. 3.8), and the high saline water can be clear differentiated from the low salinity water at depth about 75 - 115 m (Fig. 3.9). It further

proved the recirculation of high saline water from NECC to NEC. The NECC retroflex into NEC, is associated with recirculation cyclonic eddy at its northern edge (Fig. 3.8) (Hacker *et al.*, 1998).

We suspected that the cyclonic eddy at the northern NECC played an important in continuing the supply of the nutrient for the phytoplankton bloom. As a result, high chl a remained at the NWS, while the high chl a patch that extended to the west (around Sri Lanka) started to decay after the passage of the Rossby wave due to decrease nutrient supply. The cyclonic eddy will cause the lowering of SSH and doming of thermocline, which will enhance the nutrient supply into surface water. In the northern BOB, Prasanna Kumar *et al.*, (2004) suggested that eddy pumping enhances the biological productivity in that area. We speculated that the interannual variation of these eddies would affect the chl a spatial variation at NWS. However, at present stage, little is known about the occurrence of eddies at NWS and further investigation is needed.

3.5 Conclusion

This is a first hand information on the variation in chl a in SEBOB. Our study has showed the possible effects of WS and SSH to the interannual variability of chl a at SEBOB. The relationship between the high chl a and Rossby wave propagation in NWS was a new discovery. Understanding the interannual chl a variation and its relationship to the large scale atmospheric-ocean events will not only potentially contribute to predicting the fluctuation of

the fishery resources at SEBOB, but it will be an important milestone for the assessment of the tsunami effect on the primary production in this area. The possible effects of the destructive wave on the chl a variation will be address in our future research. In addition, we recommend for a detail study on the interannual variation of the currents, eddies and planetary waves in SEBOB, which could further help to explain the interannual chl a distribution pattern in this area.

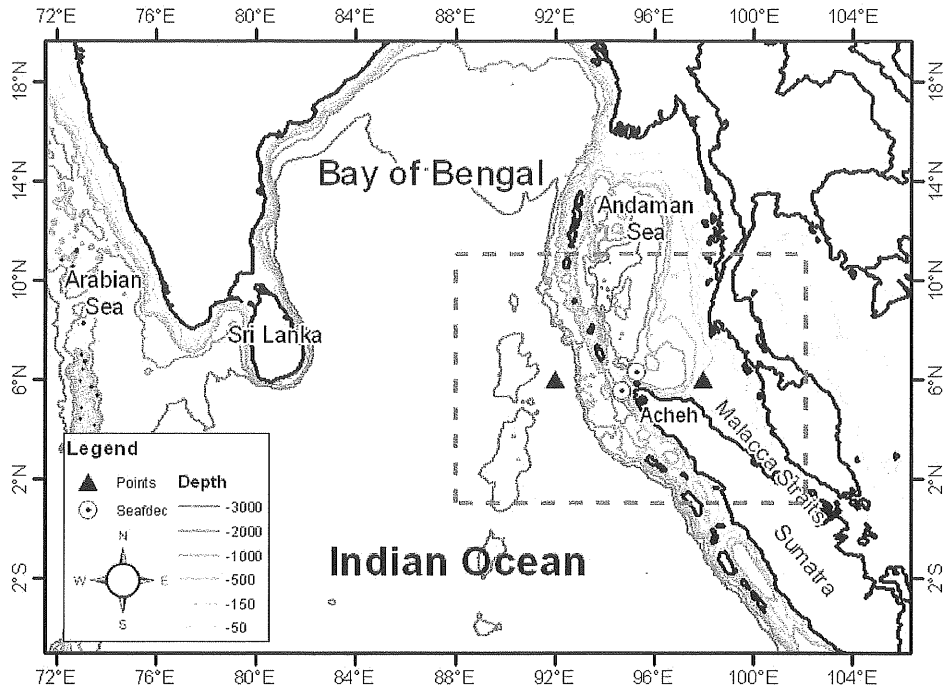

Fig. 3.1 Map of the Bay of Bengal and eastern Indian Ocean. The study area is highlighted with the box (gray dotted line). Three SEAFDEC sampling stations are shown in circle (⊙), of which two stations are located almost at the same place west of Acheh. Filled triangles (▲) show the two selected point for interannual variation analysis.

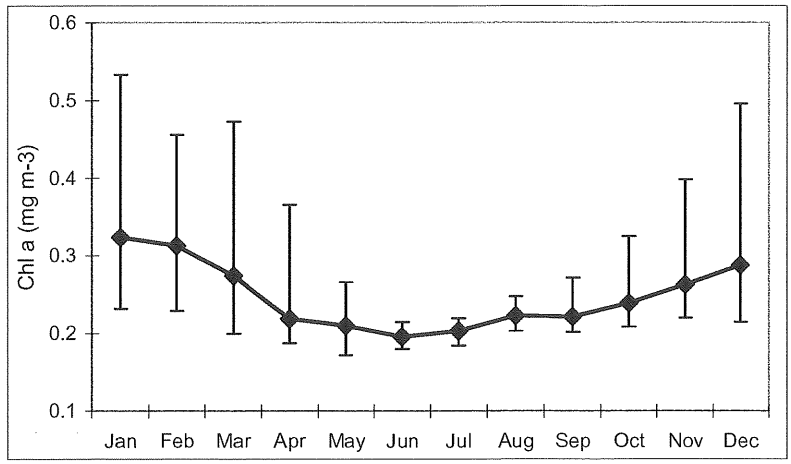

Fig. 3.2 Climatology monthly chlorophyll a (chl a) variation (mg m^{-3}) at 1.0^{o} – 10.0^{o}N 90.0^{o} – 99.0^{o}E.

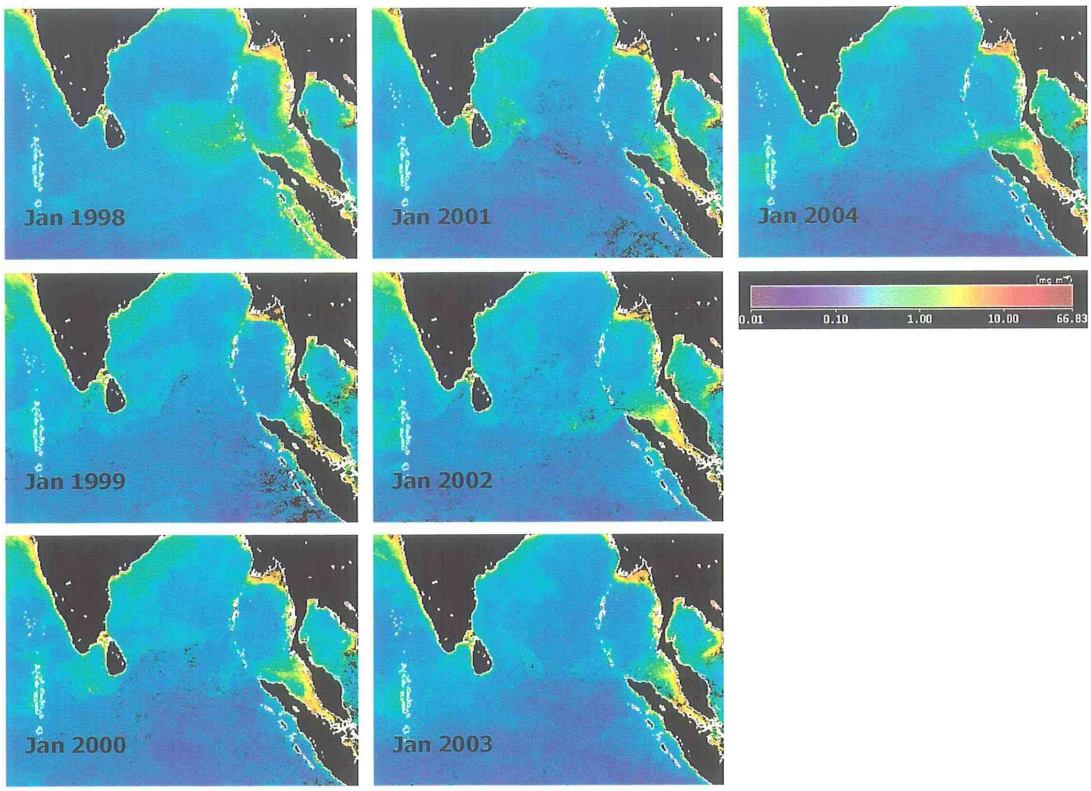

Fig. 3.3 Interannual chlorophyll a variability from January 1998 - January 2004.

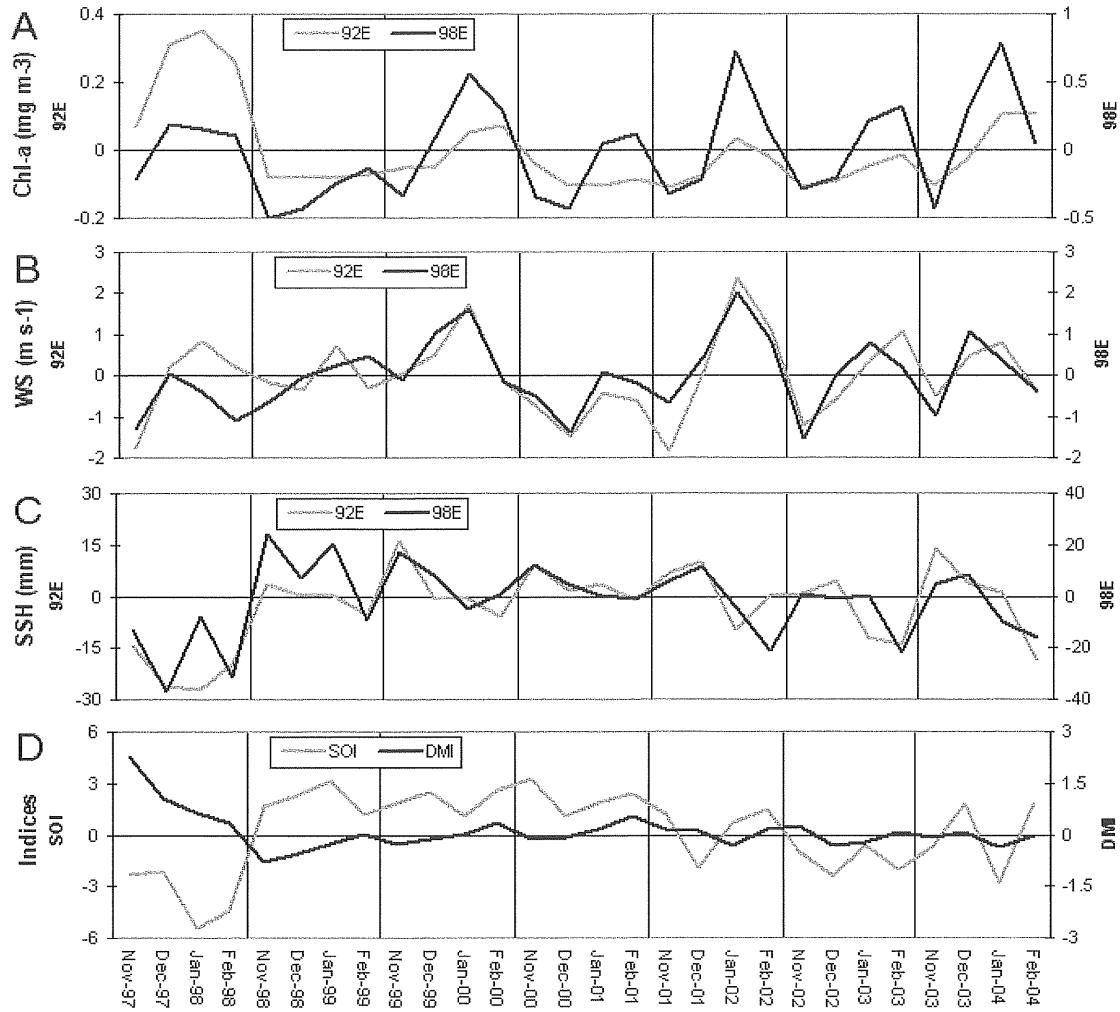

Fig. 3.4 Interannual chlorophyll a anomalies (mg m^{-3}) (A), wind speed anomalies (m s^{-1}) (B) and AVISO SSH (cm) (C) at 6.0°N 92.0°E (gray line) and 6.0°N 98.0°E (black line) during NEM from November 1997 – February 2004. DMI and SOI (D) during NEM from November 1997 – February 2004.

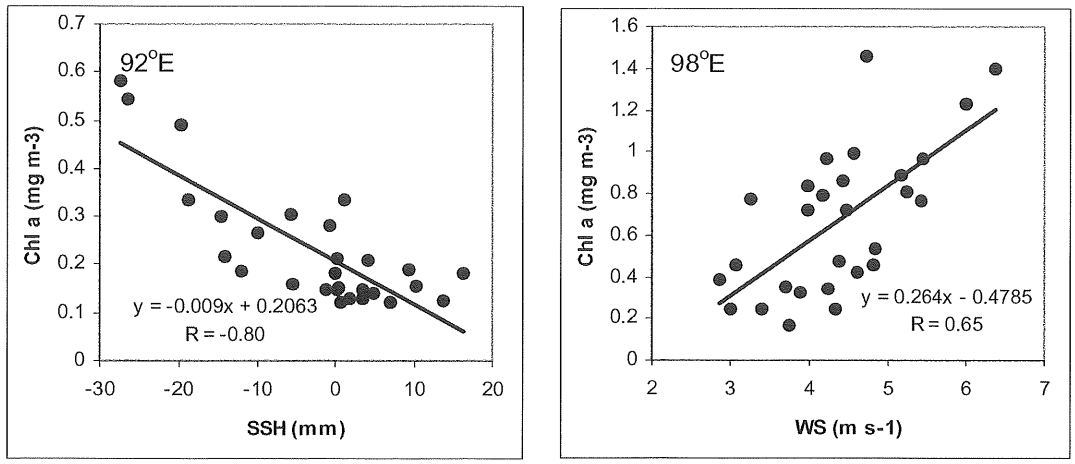

Fig. 3.5 Correlation between chlorophyll a and SSH at 92.0°E (left) and between chlorophyll a and WS at 98.0°E (right) during NEM.

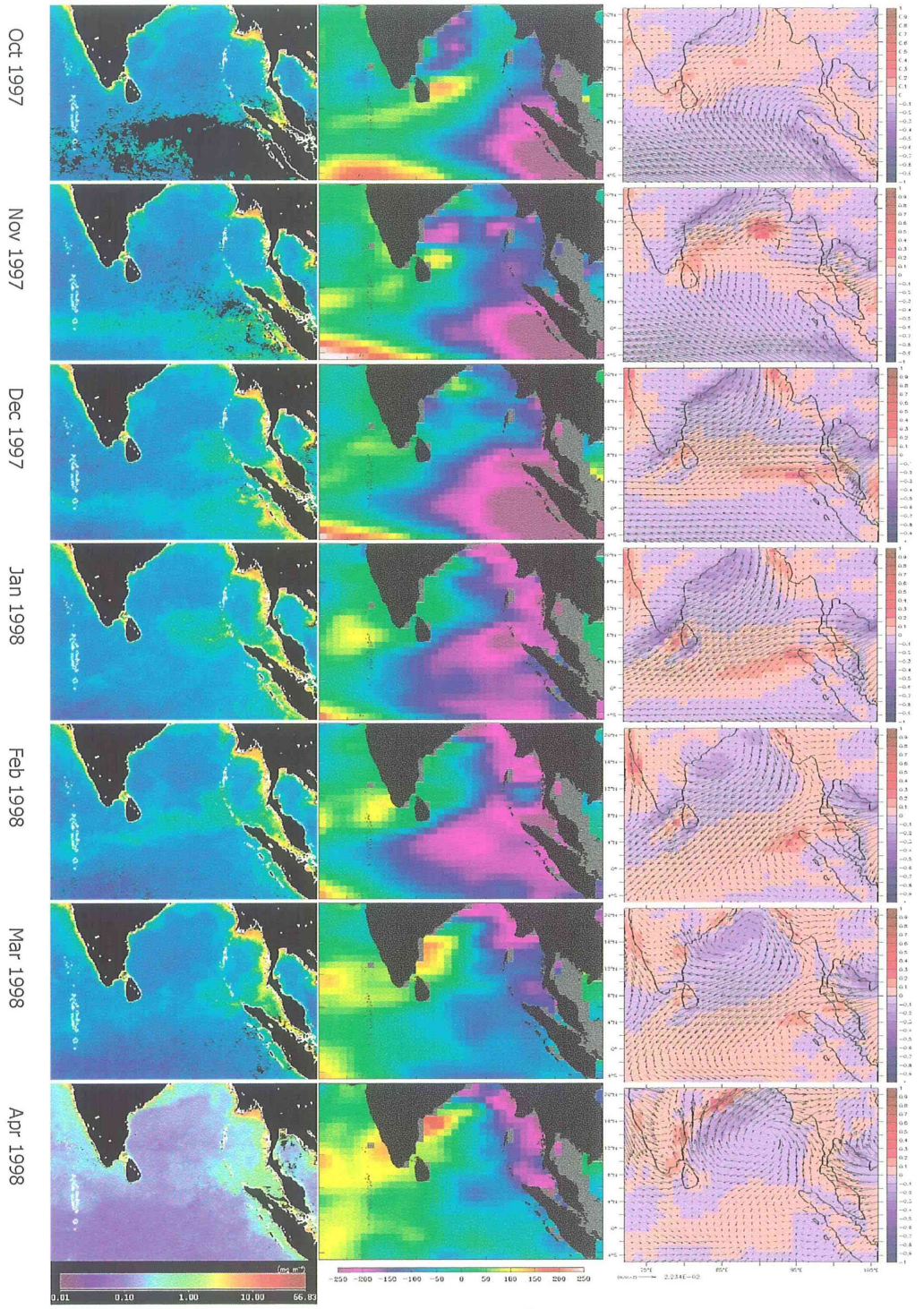

Fig. 3.6 Monthly SeaWiFS chlorophyll a (mg m^{-3}) (left), TOPEX/Poseidon SSH (mm) (middle), and FNMOC wind stress (N m^{-2}) and curl (Pa m^{-1} x 10^{-6}) (right) during October 1997 – April 1998.

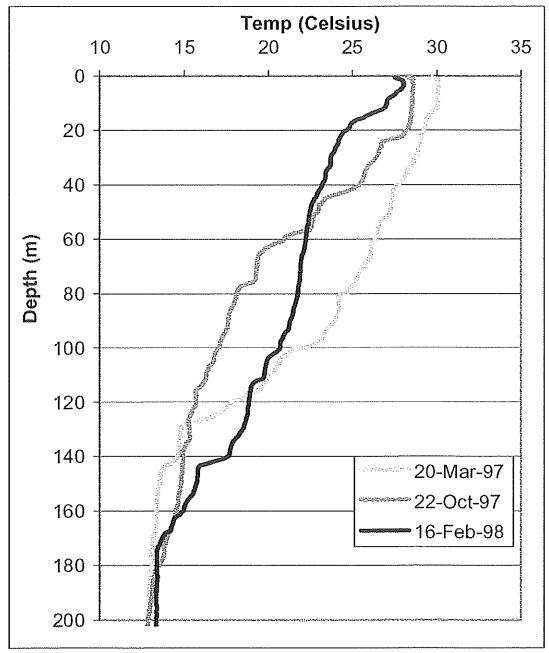

Fig. 3.7 Vertical temperature profiles (°C) near northern Sumatra before and during IOD 98. XBT data provided by SEAFDEC. Locations of the sampling points are shown in fig. 3.1, 20 March 1997 (6.3°N 95.3°E), 22 October 1997 (5.4°N 94.7°E) and 16 February 1998 (5.5°N 94.7°E).

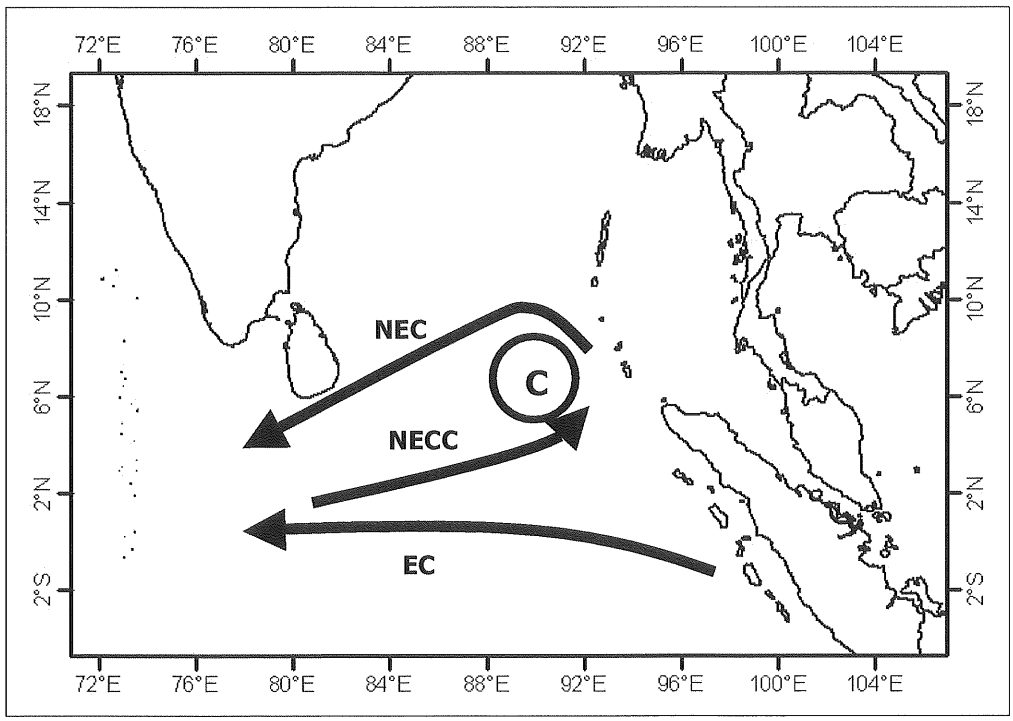

Fig. 3.8 Near-surface current during NEM (Modified after Hacker *et al.*, 1998). Current branches indicated are the North Equatorial Current (NEC), North Equatorial Counter Current (NECC), Equatorial Current (EC). Circles labeled "C" show cyclonic eddy at the eastern section of NECC.

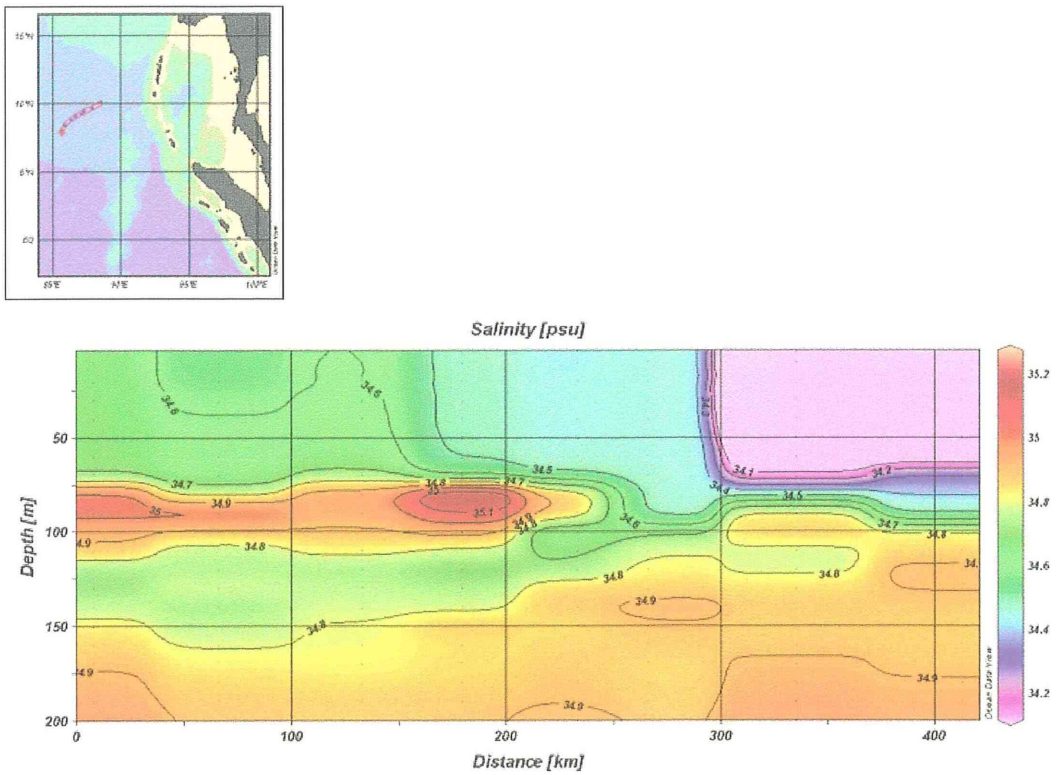

Fig. 3.9 Vertical salinity profile of ARGO float No. 2900270 from 22 December 2003 until 25 January 2004. The transect of the location is shown in the above map

Chapter 4. Assessing post tsunami effects on ocean color at eastern Indian Ocean using MODIS Aqua satellite

4.1 Introduction

On Sunday December 26, 2004, the second largest earthquake of magnitude 9.3 Richter scale hit northwestern Sumatra (Stein and Okal, 2005). The large earthquake triggered the tsunami wave that propagated throughout Indian Ocean. In less than 15 minutes, the first wave of tsunami hit the Sumatra coast (Cummins and Leonard, 2005). The force of the water is able to travel up estuarine system, often up to 6 km inland (UNEP, 2005). The tsunami runup (the maximum vertical elevation of the water on land) at western Sumatra has been recorded as high as 35 m (Tsuji, 2005). The devastation caused by tsunami was one of the worst human tragedies in history, where approximately 250000 lives have been lost (UNEP, 2005).

The eastern Indian Ocean region that badly affected by tsunami includes the Bay of Bengal (BOB), Andaman Sea and Malacca Straits (MS). There was not much study about the oceanographic conditions in this region. Due to many limitations for the in situ observations, satellite remote sensing has provided another alternative to study the oceanographic conditions in this region. Since the launching of Coastal Zone Color Scanner (CZCS) on NIMBUS-7 in 1978, ocean color remote sensing has been applied in the global ocean monitoring for more than two decades. The chlorophyll a (chl a) derived from ocean color sensor has been used as the relative measurement to phytoplankton abundance and biomass in

the ocean (Martin, 2004). In the ocean color research, the marine waters are classified into oceanic water (Case 1) and turbid water (Case 2). In the Case 1 water, all of the optical properties in the ocean are determined by the phytoplankton concentration; in Case 2 water, the optical properties are determined by various factors, such as suspended sediment, colored dissolve organic matter (CDOM) and phytoplankton concentration (Acker, 2005).

High suspended sediment in the Case 2 can be a problem for accurate chl a concentration estimation from ocean color satellite. Davis *et al.* (2000) found that the characteristic signal from suspended particular was strongest in the 550 to 600 nm spectral range. On the Sea-viewing Wide Field-of-view Sensor (SeaWiFS) sensor, the 555 nm band was good at detecting the light from suspended sediments (Acker 2005). The 551 nm band (band 12) on the Moderate-resolution Imaging Spectroradiometer (MODIS) sensor resembled the SeaWiFS 555 nm band (band 5). Li *et al.* (2003) reveal that both 551 nm and 667 nm band on MODIS can be used for sediment detection. The 551 nm band can sense far deeper into the ocean than 667 nm band because of much smaller water absorption at 551 nm than at 667 nm (Mobley, 1994). Study in the MS found that the SeaWiFS normalized water leaving radiance at 551 nm (nLw 555) value was closely related to the total suspended sediment concentration (Tan *et al.*, 2006).

The chl a and suspended sediment at the eastern Indian Ocean would show some seasonal variation where this region is strongly influenced by the Asian monsoon system. By using the SeaWiFS ocean color sensor data, Tan *et al.* (2006) reveal that the seasonal chl a

variation at the MS is higher during northeast monsoon (November – February) than southwest monsoon (May – August). Murtugudde *et al.* (1999) observed an anomalous phytoplankton bloom using SeaWiFS during October-December 1997 that coincident with anomalous upwelling off the coast of Sumatra caused by the Indian Ocean Dipole (Saji *et al.*, 1999). In the southwestern BOB, Vinayachandran and Mathew (2003) found there was a phytoplankton bloom during northeast monsoon using the Ocean Color and Temperature Scanner (OCTS) and SeaWiFS. They attributed this bloom to the open ocean upwelling driven by Ekman pumping.

Tan *et al.* (2006) found similar Ekman pumping driven upwelling event at the northern MS that caused the phytoplankton bloom during northeast monsoon. The upwelling could be one of the major factors that support the high productivity in this area. The Indian Ocean tsunami was a huge wave that have been seriously modified some of the physical environments and destructed the marine ecosystems (UNEP, 2005). However, there is no report on the effect of tsunami on phytoplankton variation. Due to the fact that the 2004 Sumatra tsunami occurred during northeast monsoon season, we are particularly interested about the tsunami effects on the upwelling event and the primary productivity. This is the first study that focused on the ocean color variation caused by the tsunami. The main objective of this study is to examine the tsunami effect on the chl a and nLw 551 variation using MODIS Aqua satellite. Besides, the meteorological variation had been examined, and its relationship to the ocean color variation was determined.

4.2 Materials and Methods

The study areas covered the tsunami affected areas at the eastern Indian Ocean with northwest limit at 10.0°N 92.0°E, and southeast limit at 0.0°N 105.0°E (Fig. 4.1). The areas consist of eastern Indian Ocean, southeastern BOB, Andaman Sea, and MS.

4.2.1 MODIS satellite data

The spatial and temporal changes of ocean color before and after the tsunami had been studied using the MODIS images. MODIS Terra and Aqua imagery were acquired from NASA Goddard Earth Science Distributed Active Archive Center (GES DAAC) and Ocean Color Web (data available at http://oceancolor.gsfc.nasa.gov/cgi/browse.pl?sen=am). Daily MODIS Aqua level 2 (1 x 1 km^2 resolution), 8 days and monthly level 3 (4 x 4 km^2 resolution) ocean color data were processed and analyzed using SeaWiFS Data Analysis System (SeaDAS). The chl a images were processed using standard MODIS chl a algorithm (OC3M). The chl a and nLw 551 data were extracted and further input into ESRI ArcGIS 8.1™ for temporal and spatial analysis.

To examine the land cover changes at western Sumatra coast, MODIS 250 m resolution RGB imagery were produced using HDFLook software. Further information about the method to create the 250m MODIS RGB images can be referred to HDFLook online manual (information available at http://www-loa.univ-lille1.fr/Hdflook/hdflook_gb.html). The generated 250 m resolution RGB images (GeoTIFF format) were later input into ArcGIS for

spatial analysis.

4.2.2 Meteorological data

To understand the meteorological effects on the ocean color variations, monthly Tropical Rainfall Measuring Mission (TRMM) accumulated rainfall data (0.25^{o} x 0.25^{o} resolution) were acquired from TRMM Online Visualization and Analysis System (TOVAS) (data available at http://lake.nascom.nasa.gov/tovas/). Daily SeaWinds Quick Scatterometer (QuikSCAT) ocean surface wind speed data (WS) (0.25^{o} x 0.25^{o} resolution) were processed and downloaded from NASA Jet Propulsion Laboratory (JPL) Physical Oceanography Distributed Active Archive Center (PO.DAAC) Ocean ESIP Tool (POET) (data available at http://poet.jpl.nasa.gov/). Fleet Numerical Meteorology and Oceanography Center (FNMOC) 6 hours WS data were downloaded from the Pacific Fisheries Environmental Laboratory (PFEL) Live Access Server (data available at http://las.pfeg.noaa.gov/las/). The 6 hours WS data were further processed into daily WS data for the comparison with daily chl a data.

4.2.3 Other data

Many of the international, governmental and commercial institution and organization has provided various Indian Ocean tsunami related data on the internet. With the cutting edge technology of the Web-based GIS, some of these data are able to be loaded into ArcGIS

ArcMap™ interface for spatial analysis on local computer. Tsunami related data has been acquired from Pacific Disaster Center (PDC) (Web GIS Server available at http://www.pdc.org), UNEP (Web GIS Server available at http:// tsunami.unep-wcmc.org), and ESRI Geography Network (Web GIS Server available at http://www.geographynetwork.com). These Web GIS data were used as additional reference in the analysis, for instance, the eroded coastline, major town etc.

4.3 Results

4.3.1 Daily surface chlorophyll a and nLw 551

4.3.1.1 Chlorophyll a

Chl a in the study areas showed large variation before and after the tsunami event on 26 December 2004 (Fig. 4.2). Before the tsunami event (13 December 2004), high chl a tongue (chl a > 5.0 mg m^{-3}) was extended from the northeastern MS toward Sumatra (Fig. 4.2). This high chl a tongue was located within the northeastern MS upwelling region. High chl a also been observed at the middle and south of MS. The chl a in MS was much higher than the eastern Indian Ocean regions that showed chl a around 0.1 – 0.5 mg m^{-3}. Slight higher chl a (chl a ~ 1.0 mg m^{-3}) was observed along the coastal water of western Sumatra.

One day after the tsunami (27 December 2004), very high chl a (chl a > 10.0 mg m^{-3}) was observed at the northwestern Sumatra (Fig. 4.2). Chl a also increased near Nias Island. The high chl a tongue at northeastern MS was disappeared, but chl a concentration still

remained high around the upwelling region. On 29 December 2004, high chl a (chl a > 8.0 mg m^{-3}) still remained at the northwestern Sumatra (Fig. 4.2) and it seemed to spread into the open ocean. Besides, higher chl a was found at the Nicobar Islands.

In the mid January (14 January 2005), the chl a along northwestern Sumatra was reduced, but still much higher than before the tsunami event (Fig. 4.2). High chl a from Singkil (2.2°N 97.8°E) and southwestern Nias Island was observed extended southward direction. Chl a along the eastern Sumatra coast was found increased, while chl a at northeastern MS still remained high.

4.3.1.2 nLw551

Similar to the chl a variation, the nLw 551 also some variation before and after the tsunami. Before the tsunami (13 December 2004), the nLw 551 values at coastal water were higher than the offshore water (Fig. 4.2). Very high nLw 551 (nLw 551 > 1.5 mW cm^{-3} μm^{-1} sr^{-1}) was observed along the eastern Sumatra coast and southern MS. Within the high chl a tongue at the northern MS, nLw 551 was slightly higher than the surrounding waters. The nLw 551 spatial distribution pattern at the upwelling area was quite similar to high chl a pattern.

On 27 December 2004, very high nLw 551 (nLw 551 > 1.5 mW cm^{-3} μm^{-1} sr^{-1}) was observed at northwestern Sumatra, which coincided with the high chl a. High nLw 551 (nLw 551 ~ 0.8 mW cm^{-3} μm^{-1} sr^{-1}) was also been found at Nias Island, and middle of Sumatra. At

the northeastern MS upwelling areas, the high nLw 551 persisted. The nLw 551 values along the center of northern MS (4.0° – 7.0°N 98.0° – 100.0°E) showed slight increased from 0.2 mW cm^{-3} μm^{-1} sr^{-1} before tsunami to 0.5 mW cm^{-3} μm^{-1} sr^{-1}. Besides, higher nLw 551 (nLw 551 ~ 0.8 mW cm^{-3} μm^{-1} sr^{-1}) was observed at the Nicobar Islands.

The high nLw 551 along western Sumatra was persisted until 14 January 2005 (Fig. 4.2). High nLw 551 at Nias Island was found extended southward that similar to the chl a pattern. Increased of nLw 551 was clearly seen along the eastern Sumatra coast. The nLw 551 at the northeastern MS and the upwelling regions was reduced.

4.3.2 Time series of surface chlorophyll a and nLw 551

The daily MODIS Aqua ocean color imagery in the previous section showed clear chl a and nLw 551 changes that could possibly attributed to the tsunami effects. However, the daily MODIS imagery is very cloudy and the quantitative variation is unclear (Fig. 4.2). In order to reduce the cloud effect and closely investigate the tsunami effect, 8 days time series of chl a and nLw 551 before and after tsunami was examined (Fig. 4.3). Ten locations distributed along the eastern Indian Ocean have been selected for this investigation. The nLw 551 data was selected using the closest available pixel to the chl a sampled location (Fig. 4.3B).

At the upwelling regions at northeastern MS (No. 2), the peak of chl a bloom (13.2 mg m^{-3}) was observed before the tsunami (10 – 17 December 2004) (Fig. 4.3A). The chl a was

slightly decreased (3.43 mg m^{-3}) during the tsunami period. During early 2005 (1 – 8 January 2005), the chl a increased again, and later decreased until February 2005.

Sudden increase of chl a during the tsunami week (26 – 31 December 2004) was observed along the Sumatra west coast up to Bandar Acheh (No. 5, 6 and 8 in fig. 4.3A). Largest increment (chl a increased about 10 times) was found at the southern of Epicenter (No. 8). The chl a at middle MS (No. 3) also found increased from 0.53 mg m^{-3} to 4.07 mg m^{-3} during tsunami, although it was protected from the direct tsunami wave by the Sumatra Island. The chl a at Nias Island (No. 9) increased about 4 times. However, chl a at the earthquake epicenter (No. 7), eastern Sumatra (No. 4), Great Nicobar Island (No. 14), and Phuket (No. 1) did not exhibit large variation neither during nor after the tsunami.

Similar to the large chl a increment during tsunami, the nLw 551 at the northwestern Sumatra (No. 5, 6 and 8) and Nias Island (No. 9) showed about two times increased of nLw 551 compared to the values before tsunami. Besides, sudden nLw 551 increased also been observed at the middle of MS (No. 3) during tsunami. The high nLw 551 at these locations was persisted a few weeks until January, which were much longer compared to the high chl a that last until end of December 2004. The nLw 551 at northern MS upwelling regions (No. 2) did not show much variation compared to the chl a. Areas at Phuket (No. 1), eastern Sumatra (No 4), epicenter (No. 7), and Nicobar Island (No. 10) did not exhibit large nLw 551 variation neither before nor after the tsunami.

In brief, the significant increment of chl a and nLw 551 was found mainly located

along the west coast of Sumatra Island and in the middle of Malacca Straits. Phuket (No. 1) and Great Nicobar Island (No. 10) that have been reported badly affected by tsunami wave did not show significant changes on the ocean color. Besides, the earthquake epicenter that located at the open ocean also showed no significant changes.

4.3.3 nLw 551 anomalies and rainfall

The 2004 tsunami had destructed some of the coastal areas, and caused high turbidity that leading to high nLw 551 values along the coastal water. To evaluate the long-term changes of the coastal water caused by the tsunami, we further examined the nLw 551 anomalies from its climatology for the period from December 2004 – April 2005. Results showed that at the northwestern Sumatra and around Bandar Acheh, positive nLw 551 anomalies about 0.2 mW cm^{-2} μm^{-1} sr^{-1} was observed in December 2004 (Fig. 4.4). This positive anomalies area persisted until January 2005. In February 2005, it became negative anomaly. Positive nLw 551 anomalies reappeared again in April 2005. This positive anomaly area was coincided with the higher rainfall (maximum 660 mm) on the land area at northwestern Sumatra in April 2005 (Fig. 4.4).

Positive nLw 551 anomalies also been observed at the eastern Sumatra coast during December 2004, January 2005 and April 2005 (Fig. 4.4). The increased nLw 551 at eastern Sumatra was also coincided with higher rainfall (maximum 550 mm). In February 2005, the maximum rainfall at eastern Sumatra sudden decreased to 110 mm, and the nLw 551

anomalies along the eastern coast showed either not much variation or negative anomaly. At the Nias Island, positive nLw 551 anomaly was observed around the island since December 2004 until February 2005. Sudden increase of nLw 551 was observed to the east of Nias Island on February 2005. The nLw 551 anomalies change to negative anomalies in April 2005. These nLw 551 anomalies changes to the east of Nias Island seem not related to the rainfall pattern at this area.

4.4 Discussions

4.4.1 The chlorophyll a variation and its over-estimation

The MODIS standard chl a algorithm (OC3M) is known to be good for the chl a prediction in oceanic water, but it will fail in turbid water. Study by Tan *et al.* (2006) at MS found that the SeaWiFS chl a algorithm (OC4v4) will have the tendency to over-estimate chl a value if the nLw 555 values is more than 1.0 mW cm^{-2} μm^{-1} sr^{-1}.

In this study, many of the increased chl a after the tsunami was coincided with higher nLw 551 values (Figs. 4.2 and 4.3). The increase of chl a at the tsunami affected coastal water could possibly due to the increase of turbidity caused by the tsunami, where the chl a value was over-estimated. Ahn *et al.* (2001) found that the presence of suspended sediment in Korean coastal waters might lead to overestimation chl a concentration up to 500%.

The sudden increase of chl a and nLw 551 did not persist for long period (Fig. 4.3). Majority of this sudden increment was probably due to the massive amounts of natural and

man-made debris that were dragged into the ocean by receding tsunami wave. In the west coast of Sumatra at Calang and Teunom, almost all above-ground infrastructures were swept into the ocean by tsunami (UNEP, 2005). The sudden increased of turbidity along the coastal water caused the over-estimation of chl a. After some period of time, the suspended sediment could be settled to the bottom or transported to other areas by the ocean wave. This could be the reason where most the chl a values returned to its normal level during early 2005 (Fig. 4.3A).

In the middle of the MS (No. 3), we suspected the increased chl a and nLw 551 (Fig. 4.3) was due to its bottom topography, which was different from the western Sumatra coast conditions where large amount of debris was dragged into the coastal water. This location is close to One Fathom Bank, where there is sudden decrease of depth that creates a physical barrier for the water exchange between the north and south MS (Liong, 1974). As the tsunami wave propagated into this shallower area, it could possibly stir up the bottom sediments as shown in the sudden increase of nLw 551. As the turbidity increased, chl a was over-estimated by the standard MODIS algorithm. Local algorithm for the chl a prediction in the turbid coastal water is needed in order to understand the actual chl a variation in this turbid water.

4.4.2. Upwelling at northeastern MS

The upwelling at northern MS plays an important role in supporting the rich marine resources not only in the MS, but also the southern Andaman Sea and northern Sumatra (Tan

et al., 2006). Tsunami wave that propagated into the MS might cause rapid mixing in this shallower area, which could stir up the bottom sediment, and causing more nutrient entrainment in the euphotic zone as shown in the middle of the straits (No. 3 in fig. 4.3). However, the nLw 551 at northern MS did not exhibit much variation before and after the tsunami event (No. 2 in fig. 4.3). This shows that the tsunami did not significantly affect the turbidity in this upwelling area.

The upwelling mechanism at northern MS is caused by monsoon wind driven Ekman pumping (Tan *et al.*, 2006). At the northern MS, there was no sudden increased of chl a soon after the tsunami, but chl a was found increased in early 2005 (Fig. 4.5). The chl a at this upwelling area increased from about 5.0 mg m^{-3} after tsunami to about 10.0 mg m^{-3} a week later. However, the QuikSCAT WS data showed that the northeast monsoon WS after tsunami (31 December 2004) was much higher than that in early 2005 (7 January 2005) (Fig. 4.5). Detail examination of the daily WS and chl a variation (Fig. 4.6) showed that the chl a at this upwelling area was rather positively related to the strength of monsoon wind with some time lag. Before the tsunami (22 – 25 December 2004), wind anomaly exhibited negative anomaly (Fig. 4.6). The chl a anomaly during 26 December 2004 – 2 January 2005 also showed negative anomaly. The relationship between WS and chl a at northern MS exhibited almost one-week time lag (Fig. 4.6). Positive wind speed anomaly was observed soon after tsunami event. The increased chl a during early 2005 could be response to this increased WS after the tsunami.

The main reason for this time lag relationship between chl a and monsoon wind could be due to the phytoplankton need some time to bloom after more nutrient is supply to the euphotic layer by wind driven upwelling. As the result, the chl a variation was closely related to the strength of the northeast monsoon winds. In brief, no clear tsunami effect on the chl a variation at northern MS, where the chl a variation was rather affected by the northeast monsoon wind.

4.4.3. Sedimentation

Some of the coastlines in the region were severely eroded by the tsunami wave. The nearshore marine ecosystem at this area is likely to have experienced direct damage from severe wave action and indirect damage from sedimentation and excessive amounts of debris (NOAA, 2005). In Andaman and Nicobar Island, the tsunami blanketed the coral reef with thick layer of silt and sands, which caused severe damage to the reef (Chakravarty, 2005). By using the 250 m resolution MODIS imagery, Joint Research Center (2005) from European Commission estimated that a total of 80795 ha of land in the Indian Ocean region were badly damaged or completely lost due to tsunami. Major changes to land cover are found along more than 1200 km of coastline, especially in Sumatra, the island north of Sumatra, the Thai Peninsular, Sri Lanka and southeastern India (Joint Research Center, 2005).

Our analysis result of MODIS 250 m RGB image before and after the tsunami also found that majority of the coastline west coast of northern Sumatra was badly affected (Fig.

4.7). The greenish coastline before the tsunami (13 December 2004) turned into brownish area after the tsunami (27 December 2004) indicated that the vegetation along the coast was totally lost after the tsunami, and caused high turbidity at the coastal water. This was the main reason of the sudden increment in chl a and nLw 551 at northwestern Sumatra coast soon after the tsunami (Fig. 4.3). As the vegetation was unable to be replaced within short period of time, these eroded coastlines were expected to be exposes direct to the ocean wave, which will cause continuous sedimentation into the ocean. The severe coastal erosion was expected to impact the coastal ecosystem in a very long period.

The sedimentation problem was found became more severe during higher rainfall, where more sediment was flushed into the ocean through the river. Besides, lack of vegetation will increase the runoff where the soil unable to retain the rainwater. This higher rainfall effects was clearly seen during April 2005 with increased nLw 551 at the northwestern Sumatra (Fig. 4.4). As the sedimentation continues, it will cause secondary damage on the already fragile marine ecosystems. On top of that, the excessive amount of debris flushed out to the sea could contained hazardous chemicals, oils, paints, freons, cleansers, etc., which could be deposited in and cause stress to nearshore environments and its living organism, like coral, seagrass, fish and other invertebrates (NOAA, 2005). Unfortunately, these impacts could be long-lived and not apparent to researchers for months or even years (NOAA, 2005).

The nLw 551 data could be applied as an important parameter for the monitoring of sedimentation condition after the tsunami event. However, our analysis results did not show

large nLw 551 variations at Phuket and Nicobar Island although severe destruction was also reported at these two locations (Fig. 4.3B). This could probably attribute to the low-resolution of nLw 551 images (4 x 4 km^2) that unable to detect the smaller scale changes over these areas. We strongly suggest that higher resolution imagery (less than 1 x 1 km^2) should be used for the assessment of the tsunami effects in these areas.

4.5 Conclusion

The Indian Ocean tsunami on 26 December 2004 had caused a vast destruction at the eastern Indian Ocean regions. This study has demonstrated that the remote sensing is a useful tool to assess the effect of tsunami on the chl a and sedimentation. By comparing the satellite image before and after the tsunami, rapid effects on the oceanographic conditions caused by the tsunami could be closely examined. High sedimentation caused by the backwash resulted in over-estimation of the chl a values by ocean color satellite. However, the chl a at the upwelling area at northern MS did not exhibit any significant changes from the tsunami wave. The chl a bloom at this upwelling area was mainly driven by the northeast monsoon wind. At the seriously eroded coastline along western Sumatra, continuous sedimentation was observed. Sedimentation became more severe during higher rainfall due to the surface vegetations were destructed by the tsunami. This sedimentation problem will cause impact on the coastal marine ecosystem, where the future of marine resources in the region could be dramatically affected, especially the fishery and tourism industries. We strongly recommended that the sedimentation

problem being monitored for a longer period, where this information could be beneficial for the assessment of long-term effects on the marine ecosystem.

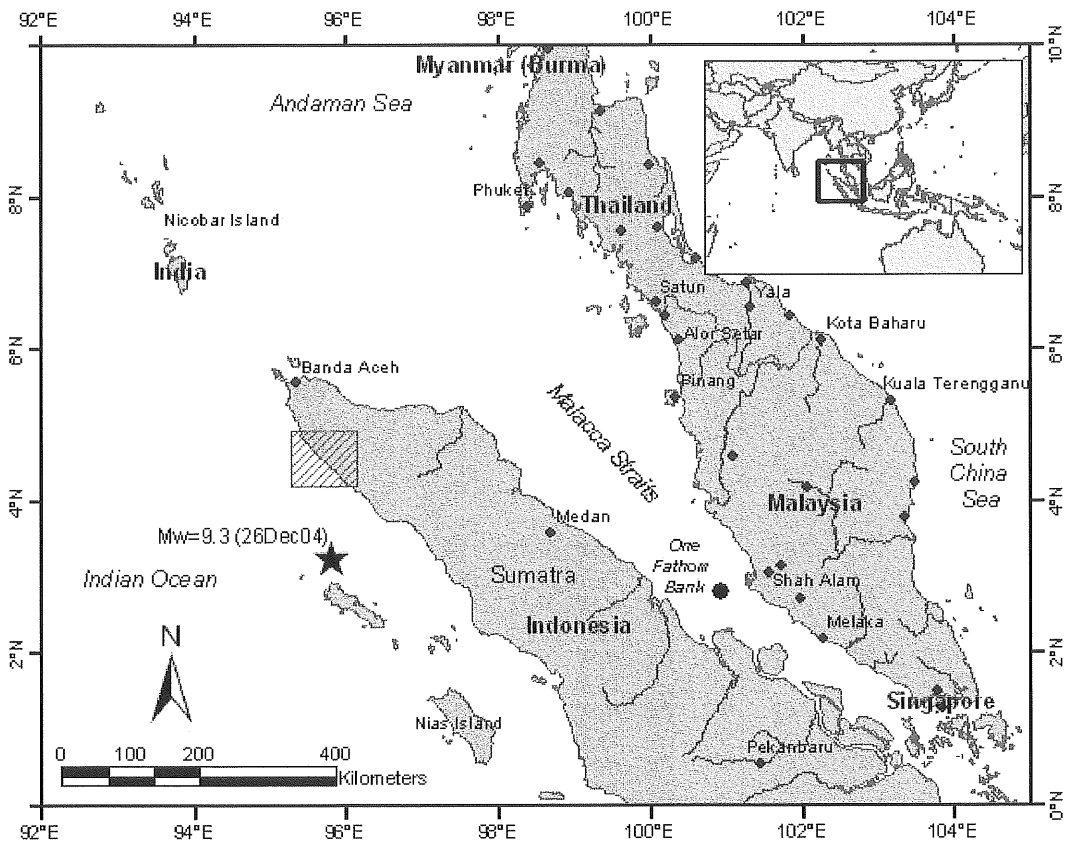

Fig. 4.1 Area of study. The star shows the location of earthquake epicenter on 26 December 2004. Dark marker at the center of Malacca Straits indicates the location of One Fathom Bank. The gray box at northwestern Sumatra shows the images location on fig. 4.7.

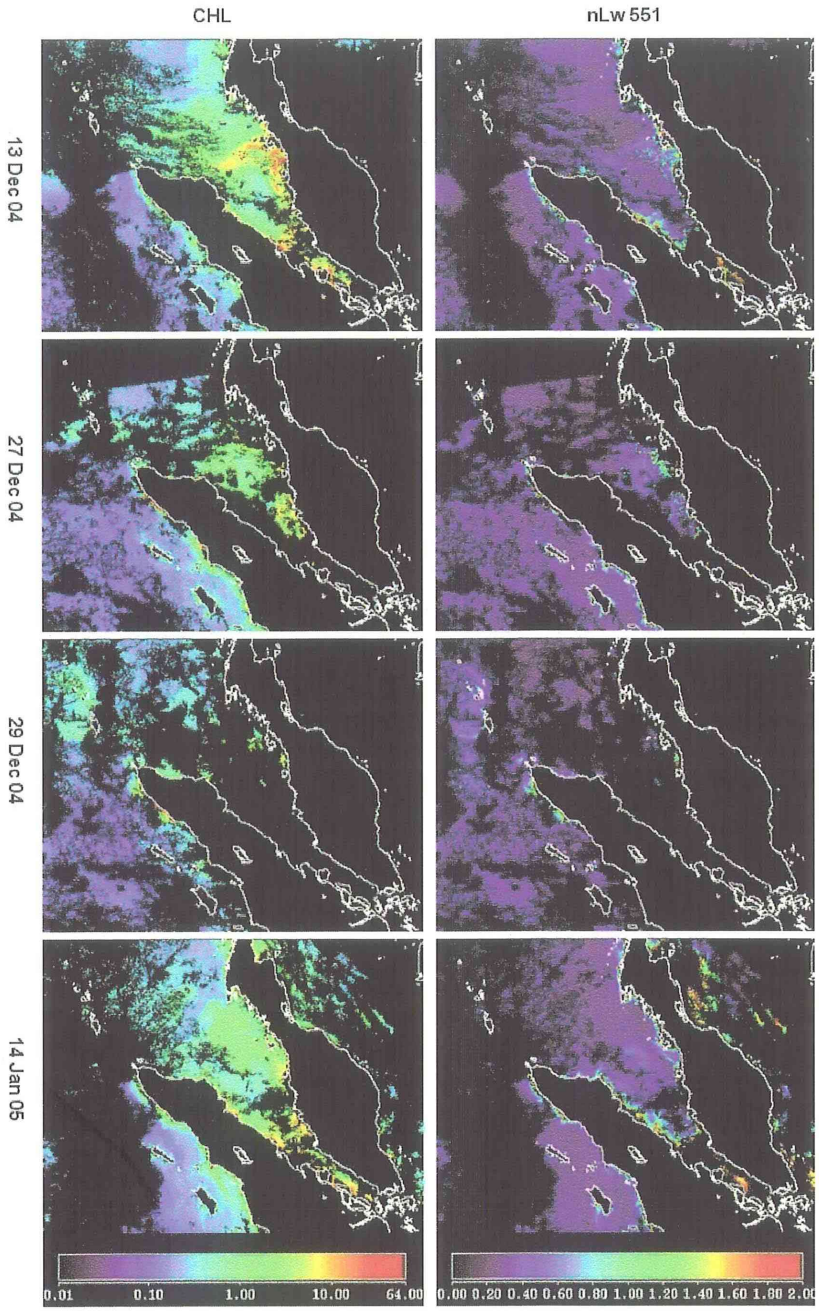

Fig 4.2 Chlorophyll a (chl a) (left column) (mg m^{-3}) and nLw 551 (right column) (mW cm^{-2} μm^{-1} sr^{-1}) before and after the tsunami. Coastline is shown in white line. Cloud or erroneous data are masked in black color.

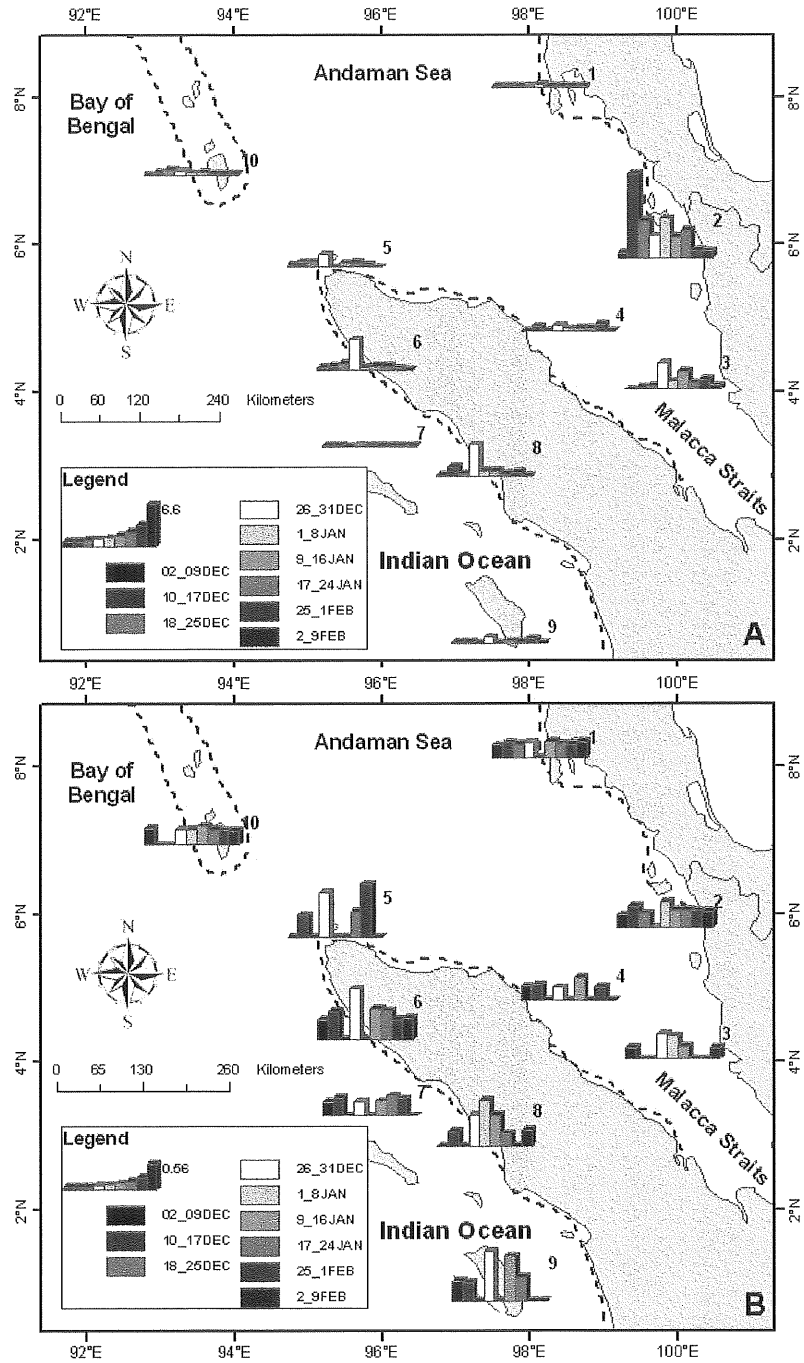

Fig. 4.3 MODIS chlorophyll a (A) (mg m^{-3}) and nLw 551 (B) (mW cm^{-2} μm^{-1} sr^{-1}) 8 days variation before and after tsunami for selected locations. Dotted lines show tsunami affected coasts.

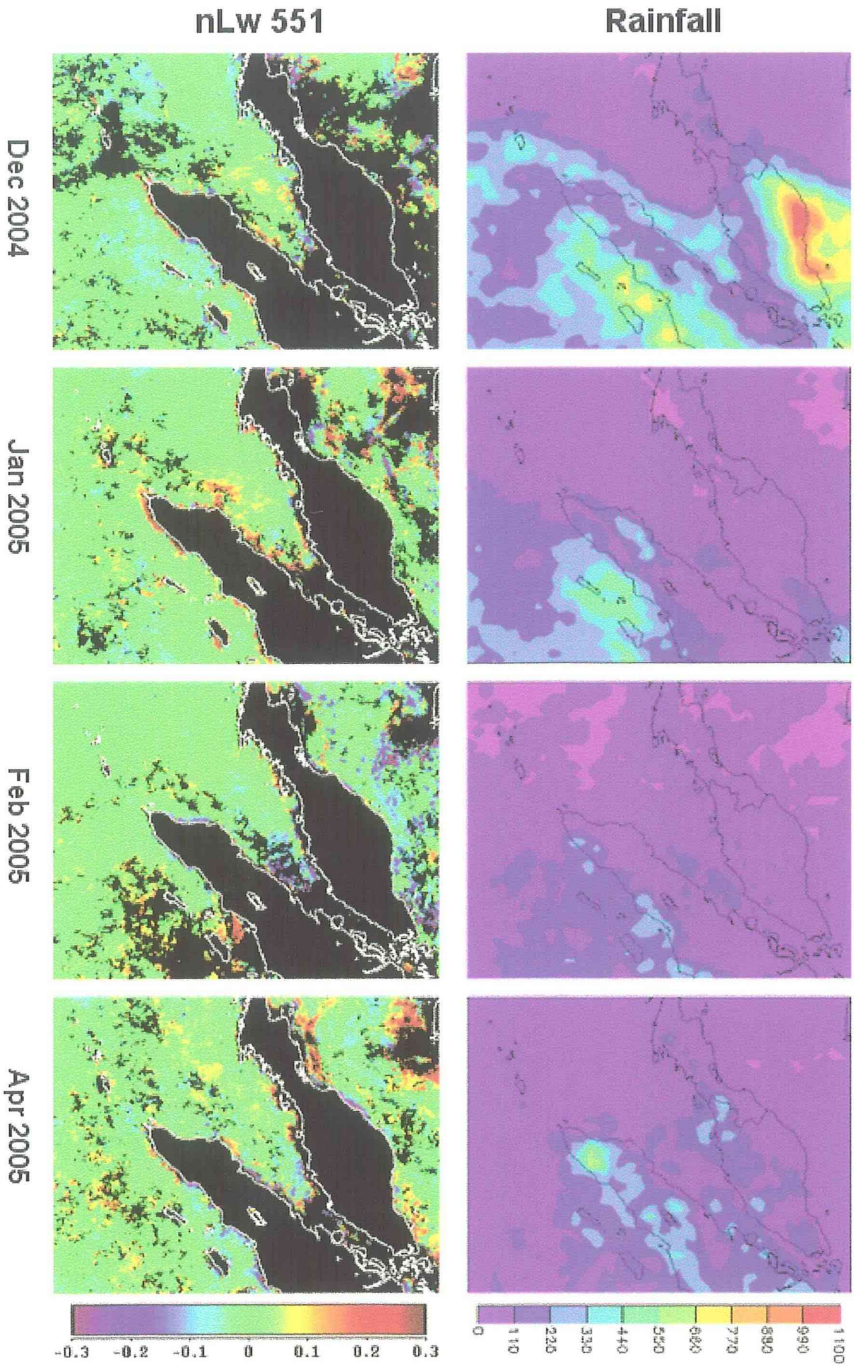

Fig. 4.4 Differences of monthly nLw 551 (left column) (mW cm^{-2} μm^{-1} sr^{-1}) from the nLw551 climatology, and TRMM accumulated rainfall (right column) (mm) during December 2004 – April 2005. Coastline of nLw 551 is shown in white line, while coastline for rainfall is shown in black line. The cloudy or erroneous data in nLw 551 images are masked with black color.

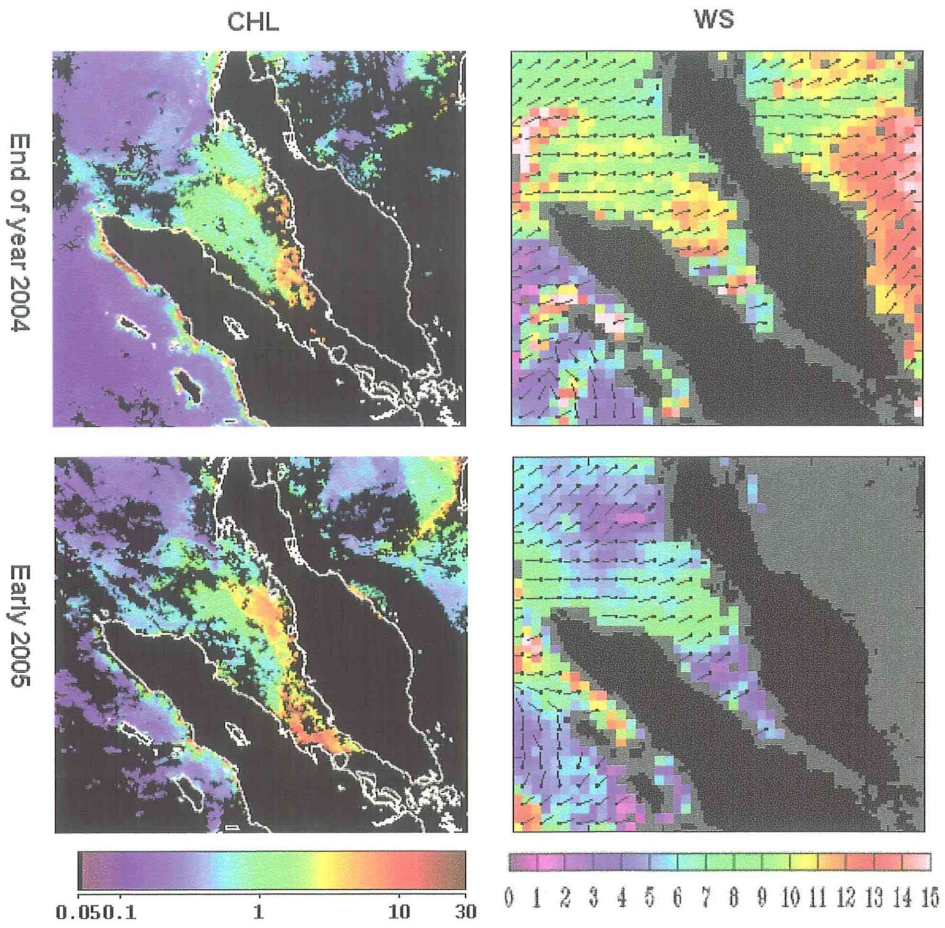

Fig. 4.5 MODIS 8 Days chlorophyll a (chl a) (mg m^{-3}) (left) and daily QuikSCAT wind vector and wind speed (WS) (m s^{-1}) (right).

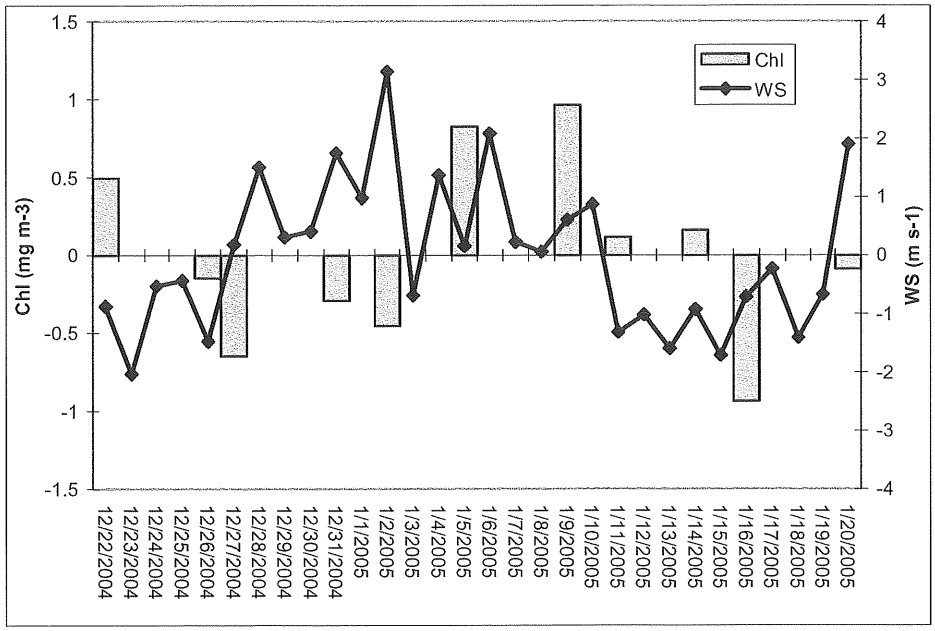

Fig. 4.6 Daily wind speed (WS) (m s^{-1}) and chlorophyll a (chl a) (mg m^{-3}) at northern MS (6.0°N 99.0°E).

Fig. 4.7 MODIS true color 250m RGB image for northern Sumatra (left) on 13 December 2004 before the tsunami (left) and MODIS image on 29 December 2004 after the tsunami (right). The location of these images is shown in fig. 4.1. The coastal areas at this northwestern Sumatra Island were badly destructed by the tsunami wave on 26 December 2004.

Chapter 5. General Conclusion

Ocean color remote sensing technology has been proven as an effective technique that enables the monitoring of the oceanographic conditions in more synoptic and comprehensive way. This study has provided the insight of the seasonal and interannual chl a variation at the eastern Indian Ocean. It started from a smaller area at MS, and then further extended the study throughout the eastern Indian Ocean region. By understanding the factors that contribute to seasonal and interannual chl a variation at the regions, we were able to further examine the 2004 tsunami effects on the ocean color and marine environment.

There are a few new and significant findings in this preliminary study in the eastern Indian Ocean region. The chl a variation in the region was found closely related to the monsoon and large-scale atmospheric-oceanographic dynamics. By using the continuous monitoring from ocean color images, we discovered the upwelling event during NEM and downwelling event during SWM in northern MS. The special topography in MS has enabled both upwelling and downwelling occurred over the same area during different monsoon season.

To the east of MS in the deep Indian Ocean, we found that the interannual chl a variation is related to the variation of monsoon wind and SSH. Besides, we discovered that there was an open ocean phytoplankton bloom that related to Rossby wave propagation during the IOD 1997 - 98. The Low SSH Rossby wave caused shoaling of thermocline and nutrient entrainment that initiated phytoplankton bloom. However, the influences of Kelvin

wave, surface current system and eddies at eastern Indian Ocean on the chl a variation are still unclear at present study. We hope to address the variability of these factors in the future work.

The 2004 Indian Ocean Tsunami has been reported changing the marine environment at the affected areas. However, our study showed that there were no significant effects on the upwelling at northern MS, except a few coastal areas along the eastern Indian Ocean that were badly destroyed by the huge wave. The nLw 555 on SeaWiFS and nLw 551 on MODIS is a good indicator for the turbid water and erroneous chl a estimation. Our study proven that these parameters can be applied for the monitoring of the sedimentation problem by the tsunami. To monitor the tsunami effects on a smaller area, we suggested that higher resolution imagery should be used.

The findings from this research will be very helpful for the marine resources and coastal zone management. The information on the scale of upwelling and phytoplankton bloom can be applied for the prediction of fishery resource fluctuation. Together with the information of fish landing, the fishery authorities will be able to determine the suitable fishes landing limits for a sustainable yield of fisheries management. On top of that, the ocean color remote sensing is also capable to monitor the eutrophication and sedimentation problems in the study area. We suggested that long term monitoring using the ocean color satellite and in-situ study should be carried out in order to examine changes of the marine environment in this region.

References

Acker, J. (2005): Sedimentia. Available online at http://daac.gsfc.nasa.gov/oceancolor/sedimentia.shtml (access 20 July 2005).

Ahn, Y. H., J. E. Moon and S. Gallegos (2001): Development of suspended particulate matter algorithms for ocean color remote sensing. *Korean Journal of Remote Sensing,* **17** (4), 285-295.

Asanuma, I. K. Matsumoto, H. Okana, T. Kawano, N. Hendiatri and S. I. Scahoemar (2003): Spatial distribution of phytoplankton along the Sunda Islands: The monsoon anomaly in 1998. *J. Geophys. Res.,* **108**(C6), 3202, doi:10.1029/1999JC000139.

Banglapedia (2005): Bay of Bengal. Available online at http://banglapedia.search.com.bd/HT/B_0361.HTM (access 22 August 2005).

Bauer, S., G. L. Hitchcock and D. B. Olson (1991): Influence of monsoonally-forced Ekman dynamics upon surface layer depth and plankton biomass distribution in the Arabian Sea. *Deep Sea Res.*, **38**, 531– 553.

Brock, J., C. McClain, M. Luther and W. Hay (1991): The phytoplankton bloom in the northwestern Arabian Sea during the southwest monsoon of 1979. *J. Geophys. Res.*, **96**, 20,623– 20,642.

Chakravarty, P. (2005): News in Science – Tsunami dumped tonnes of sediment on reef. Available online at http://www.abc.net.au/cgi-bin/common/printfriendly.pl?/science/news/stories/s1364070.htm (accessed 1 June 2005).

Chua, T. E., I. R. L. Gorre, S. A. Ross, S. R. Bernad, B. Gervacio and M. C. Ebarvia (2000): The Malacca Straits. *Mar. Pollut. Bull.*, **41**(1-6), 160-178.

Chua, T. E., S. A. Ross and H. M. Yu (Eds.) (1997): *Malacca Straits environmental profile,* MPP-EAS Technical Report 10, GEF/UNDP/IMO Regional Programme for the Prevention and Management of Marine Pollution in the East Asian Seas, Quezon City, Philippines, 259 pp.

Church, J. A., J.-P. Bethoux and A. Theocharis (1998): Semienclosed seas, islands and Australia coastal segment. p. 79 – 101. In *The Sea,* Volume 11, ed. by A. R. Robinson and K. H. Brink, John Wiley and Sons, New York.

Cipollini, P., D. Cromwell, P. Challenor and S. Raffaglio (2001): Rossby waves detected in global ocean colour data. *Geophys. Res. Lett.*, **28**, 323-326.

Cummins, P. and M. Leonard (2005): The Boxing Day 2004 tsunami- A repeat of 1833?. Available online at http://www.ga.gov.au/image_cache/GA5892.pdf (accessed 11 November 2005).

Davis, C. O., J. T. O. Kirk, J. S. Parlow and S. Sathyendranath (2000): Measurement requirements for Case 2 waters. p. 77-91. In *Remote Sensing of Ocean Color in Coastal, and Other Optically-complex, Waters*, Reports of the International Ocean-Color Coordinating Group, No. 3, ed. by S. Sathyendranath, IOCCG, Darthmouth.

Dey, S. and R. P. Singh (2003): Comparison of chlorophyll distributions in the northeastern Arabian Sea and southern Bay of Bengal using IRS-P4 Ocean Color Monitor Data. *Remote Sen. Environ.,* **85**, 424-428.

Fairbridge, R. W. (Ed.) (1966): *The Encyclopedia of Oceanography*. Encyclopedia of Earth Sciences Series, Van Nostrand Reinhold Company, New York, 1021 pp.

Gomes, H. R., J. I. Goes and T. Saino (2000): Influence of physical processes and freshwater discharge on the seasonality of phytoplankton regime in the Bay of Bengal. *Cont. Shelf Res.*, **20**, 313-330.

Hacker, P., E. Firing, J. Hummon, A. L. Gordon and J. C. Kindle (1998): Bay of Bengal currents during the northeast monsoon. *Geophys. Res. Lett.*, **25** (15), 2769-2772.

Han, W. Q. and P. J. Webster (2002): Forcing Mechanism of Sea Level Interannual Variability in the Bay of Bengal. *J. Phys. Oceanogr.*, **32**, 216-239.

Hendiarti, N., H. Siegel and T. Ohde (2004): Investigation of different coastal processes in Indonesian waters using SeaWiFS data. *Deep-Sea Res. II,* **51**, 85-97.

IOCCG (1999): *Status and Plans for Satellite Ocean-Colour Missions: Considerations for Complementary Missions*, ed. by J. A. Yoder, Reports of the International Ocean-Colour Coordinating Group, No. 2, IOCCG, Dartmouth, Canada, 43 pp.

IOCCG (2000): *Remote Sensing of Ocean Colour in Coastal, and Other Optically-Complex, Waters*, ed. by Sathyendranath, S., Reports of the International Ocean Colour Coordinating Group, No. 3, IOCCG, Dartmouth, Canada, 140 pp.

Ittekkot, V., H. R. Kudrass, D. Quadfasel and D. Unger (eds.) (2003): The Bay of Bengal –An Introduction. *Deep-Sea Res. II*, **50**, 853-854.

Joint Research Centre (2005): Mapping severe damage to S. E. Asia's land cover following the tsunami. Available online at http://tsunami.jrc.it/Reports/Tsunami_land_cover_change.pdf (accessed 1 June 2005).

Kasyapa, K. (2000): Seasonal variability of sea surface chl arophyll-a of waters around Sri Lanka. *Proc. Indian Acad. Sci. (Earth Planet Sci.),* **109** (4), 427-432.

Kumar, S. P., P. M. Muraleedharan, T.G. Prasad, M. Gauns, N. Ramaiah, S. N. de Souza, S. Sardesai and M. Madhupratap (2002): Why is the Bay of Bengal less productive during summer monsoon compared to the Arabian Sea? *Geophys. Res. Lett.*, **29**(D24), 2235, doi:10.1029/2002GL016013.

Lee, C., B. Jones, K. Brink and A. Fischer (2000): The upper-ocean response to monsoonal forcing in the Arabian Sea: seasonal and spatial variability. *Deep-Sea Res. II*, **47**, 1177– 1226.

Li, R. R., Y. J. Kaufman, B. C. Gao and C. O. Davis (2003): Remote sensing of suspended sediments and shallow coastal waters. *IEEE T. Geosci. Remote.*, **41**(3), 559-566.

Lierheimer, L. J. and K. Banse (2002): Seasonal and interannual variability of phytoplankton pigment in the Laccadive (Lakshadweep) Sea as observed by the Coastal Zone Color Scanner. *Proc. Indian Acad. Sci.* (Earth. Planet. Sci.), **111**, 163– 185.

Limpsaichol, P. (2005): Oceanographic features with biological indication in the Andaman Sea, Thailand. Available online at http://sol.oc.ntu.edu.tw/omisar/wksp.mtg/wom2.98a/np/6E_PRAWEEN.html (access 22 August 2005).

Liong, P. C. (1974): Hydrography of the Strait of Malacca. *Malaysian Agriculture Journal*, **49**(3), 381-391.

Liu, K. K., S. Y. Chao, P. T. Shaw, G. C. Gong, C. C. Chen and Y. T. Tang (2002): Monsoon-forced chlorophyll distribution and primary production in the South China Sea: observations and a numerical study. *Deep-Sea Res. I,* **49**, 1387-1412.

Madhupratap, M., M. Gauns, N. Ramaiah, S. P. Kumar, P. M. Muraleedharan, S. N. de Souza, S. Sardesai and U. Muraleedharan (2003): Biogeochemistry of the Bay of Bengal: Physical, chemical and primary productivity characteristics of the central and western Bay of Bengal

during summer monsoon 2001. *Deep Sea Res. II*, **50**, 881– 896.

Malaysian Meteorological Service (2005): Monsoon: Changing Winds. Available online at http://www.kjc.gov.my/english/education/weather/monsoon01.html (access 31 August 2005).

Martin, S. (2004): *An Introduction to Ocean Remote Sensing*. Cambridge University Press, Cambridge, p. 124-165.

McClain, C. R., J. R. Christian, S. R. Signorini, M. R. Lewis, I. Asanuma, D. Turk and C. Dupouy-Douchement (2002): Satellite ocean-color observations of the tropical Pacific Ocean. *Deep-Sea Res. II*, **49**, 2533-2560.

McCreary, J. P., H. S. Lee and D. B. Enfield (1989): The response of the coastal ocean to strong offshore winds; with application to circulations in the Gulfs of Tehuantepec and Papagayo. *J. Mar. Res.*, **47**, 81-109.

McCreary, J. P., Jr. K. E. Kohler, R. R. Hood and D. B. Olson (1996): A four-component ecosystem model of biological activity in the Arabian Sea. *Progress in Oceanogr.*, **37**, 193–240.

McGillicuddy, D. J., A. R. Robinson, D. A. Siegel, H. W. Jannasch, R. Johnson, T. D. Dickey, J. McNeil, A. F. Michaels and A. H. Knap (1998): Influence of mesoscale eddies on new production in the Sargasso Sea. *Nature*, **394**, 263-266.

Mobley, C. D. (1994): *Light and Water Radiative Transfer in Natural Waters*. Academic Press, New York, p. 80-100.

Murtugudde, R. G., S. R. Signorini, J. R. Christian, A. J. Busalacchi, C. R. McClain and J. Picaut (1999): Ocean color variability of the tropical Indo-Pacific basin observed by SeaWiFS during 1997-1998. *J. Geophys. Res.*, **104**(C8), 18351-18366.

NOAA (National Oceanic and Atmospheric Administration) (2005): Potential ecological impacts of Indian Ocean tsunami on nearshore marine ecosystem. Available online at http://www.noaanews.noaa.gov/stories2005/s2362.htm (access 15 April 2005).

Namba, T. and H. M. Ibrahim (2002): Mixed layer depth in the Straits of Malacca. p. 269-279. In *Tropical Marine Environment: Charting Strategies for the Millennium*, ed. by F. M. Yusoff, M. Shariff, H. M. Ibrahim, S. G. Tan and S. Y. Tai, Malacca Straits Research and Development Centre (MASDEC), University Putra Malaysia, Serdang, Malaysia.

Prasanna Kumar, S., M. Madhupratap, M. Dileep Kumar, P. M. Muraleedharan, S. N. de Souza, M. Gauns and V. V. S. S. Sarma (2001): High biological productivity in the central Arabian Sea during summer monsoon driven by Ekman pumping and lateral advection. *Curr. Sci.*, **81**, 1633– 1638.

Prasanna Kumar, S., M. Muraleedharan, T. G. Prasad, M. Gauns, N. Ramaiah, S. N. de Souza, S. Sardesai and M. Madhupratap (2002): Why is the Bay of Bengal less productive during summer monsoon compared to the Arabian Sea?. *Geophys. Res. Lett.*, **29**(24), 2235.

Prasanna Kumar, S., M. Nuncio, J. Narvekar, A. Kumar, S. Sardesai, S. N. de Souza, M. Gauns, N. Ramaiah and M. Madhupratap (2004): Are eddied nature's trigger to enhance biological productivity in the Bay of Bengal. *Geophys. Res. Lett.*, **31**, L07309, doi:10.1029/2003GL019274.

Rao, S. A., V. V. Gopalakrishna, S. R. Shetye and T. Yamagata (2002): Why were cool SST anomalies absent in the Bay of Bengal during the 1997 Indian Ocean Dipole Event?. *Geophys. Res. Lett.*, **29** (11), 1555.

Robinson, I. S. (2004): *Measuring the Oceans from Space: The principles and methods of satellite oceanography*. Springer-Verlag, Berlin, p. 149-241.

Saji, N. H., B. N. Goswami, P. N. Vinayachandran and T. Yamagata (1999): A dipole mode in the tropical Indian Ocean. *Nature*, **401**, 360-363.

Satish, R. S. and A. D. Gouveia (1998): Coastal circulation in the north Indian Ocean. p. 523-556. In *The Sea*, Vol. 11, ed. by A. R. Robinson and K. H. Brink, John Wiley and Sons, New York.

Secchi, P. A. (1866): Esperimento per determinare la transparanza del mare. p. 258-288. In *Sul Moto Ondoso del Mare*, ed. by A. Cialdi, Rome.

Setiapermana, D., E. Triyati and A. Nontji (1984): Pengamatan klorofil dan seston di perairan Selat Melaka, 1978-1980. p. 63-66. In *Evaluasi kondisi perairan Selat Melaka, 1978-1980*, ed. by M. K. Moosa, D. P. Praseno and W. Kastoro, Lembaga Oseanologi Nasional, Jakarta, Indonesia. (in Indonesian).

Shetye, S. R., A. D. Gouveia, S. S. C. Shenoi, D. Sundar, G. S. Michael, A. M. Almeida, and K. Santanam (1990): Hydrography and circulation off the west coast of India during the southwest monsoon 1987. *J. Mar. Res.*, **48**, 359– 378.

Siegel, D. A. (2001): The Rossby rototiller. *Nature*, **409**, 576-577.

Stein, S. and E. A. Okal (2005): Speed and size of the Sumatra earthquake. *Nature*, **434**, 581-582.

Susanto, R. D., A. L. Gordon and Q. Zheng (2001): Upwelling along the coast of Java and Sumatra and its relation to ENSO. *Geophys. Res. Lett.*, **28**, 1599-1602.

Tan, C. K., J. Ishizaka, S. Matsumura, F. M. Yusoff and M. I. Mohamed (2006): Seasonal variability of SeaWiFS chlorophyll a in the Malacca Straits in relation to Asian monsoon. *Cont. Shelf Res.*, **26**, 168-178.

Tang, D. L., H. Kawamura, T. V. Dien and M. A. Lee (2004): Offshore phytoplankton biomass increase and its oceanographic causes in the South China Sea. *Mar. Ecol. Prog. Ser.*, **268**, 31-41.

Tang, D. L., I. H. Ni, D. R. Kester and F. E. Müller-Karger (1999): Remote sensing observation of winter phytoplankton blooms southwest of the Luzon Strait in the South China Sea. *Mar. Ecol. Prog. Ser.*, **191**, 43– 51.

Tang, D. L., I. H. Ni, F. E. Müller-Karger and Z. J. Liu (1998): Analysis of annual and spatial patterns of CZCS-derived pigment concentrations on the continental shelf of China. *Cont. Shelf Res.*, **18**, 1493– 1515.

Tomczak, M. and J. S. Godfrey (2002): *Regional Oceanography: An Introduction*. Available online at http://www.es.flinders.edu.au/~mattom/regoc/pdfversion.html (access 30 August 2005).

Tsuji, Y. (2005): Distribution of the tsunami heights of the 2004 Sumatra tsunami in Bandar Acheh measured by the Tsunami Survey Team. Available online at http://www.eri.u-tokyo.ac.jp/namegaya/sumatera/surveylog/edata.htm (accessed 30 June 2005).

UNEP (United Nation Environment Programme) (2005): After the tsunami: Rapid environmental assessment. Available online at http://www.unep.org/tsunami/tsunami_rpt.asp (accessed 1 June 2005).

Uktolseya, H. (1988): Physical and biological characteristics of the Straits of Malacca in the framework of coastal management. p. 118-131. In *Coastal zone management in the Straits of*

Malacca, Proceeding of a Symposium on the Environmental Research and Coastal Zone Management in the Straits of Malacca, School for Resource and Environmental Studies, Dalhousie University, Halifax, Nova Scotia.

Uz, B., J. Yoder and V. Osychny (2001): Pumping of nutrients to ocean surface waters by the action of propagating planetary waves. *Nature*, **409**, 597-600.

Vinayachandran, P. N. and S. Mathew (2003): Phytoplankton bloom in the Bay of Bengal during the northeast monsoon and its intensification by cyclones. *Geophys. Res. Lett.*, **30** (11), 1572, doi:10.1029/2002GL016717.

Vinayachandran, P. N., P. Chauhan, M. Mohan and S. Nayak (2004): Biological response of the sea around Sri Lanka to summer monsoon. *Geophys. Res. Lett.*, **31**, L01302, doi:10.1029/2003GL018533.

Wang, D., Q. Xie, Y. Du, W. Q. Wang and J. Chen (2002): The 1997-1998 warm event in the South China Sea. *Chin. Sci. Bull.*, **47**, 1221-1227.

Webster, P. J., A. M. Moore, J. P. Loschnigg and R. R. Leben (1999): Coupled ocean-atmosphere dynamics in the Indian Ocean during 1997-98. *Nature*, **401**, 356-360.

Wikipedia (2005A): Andaman Sea. Available online at http://en.wikipedia.org/wiki/Andaman_Sea (access 23 August 2005).

Wikipedia (2005B): Indian Ocean. Available online at http://en.wikipedia.org/wiki/Indian_Ocean (access 12 August 2005).

Wikipedia (2005C): Straits of Malacca. Available online at http://en.wikipedia.org/wiki/Malacca_Straits (access 23 August 2005).

Wilson, C. and D. Adamec (2002): A global view of bio-physical coupling from SeaWiFS and Topex satellite data, 1997-2001. *Geophys. Res. Lett.*, **29** (8), 1257.

Wyrtki, K. (1961): Scientific results of marine investigation of the South China Sea and the Gulf of Thailand 1959-1961. In *Physical oceanography of Southeast Asian waters*, Naga Report II, vol. 2. Scripps Institute of Oceanography, University of California, La Jolla, 195 pp.

Wyrtki, K. (1987): Indonesian throughflow and the associated pressure gradient. *J. Geophys. Res.*, **92**, 12941-12946.

Xie, S. P., Q. Xie, D. X. Wang and W. T. Liu (2003): Summer upwelling in the South China Sea and its role in regional climate variations. *J. Geophys. Res.*, **108** (C8), 3261, doi:10.1029/2003JC001867.

Yesaki, M. and P. Jantarapagdee (1981): Wind stress and temperature changes off the west coast of Thailand. *Phuket Mar. Biol. Cent. Res. Bull.*, **28**, 27-41.

Yoder, J. A. and M. A. Kennelly (2003): Seasonal and ENSO variability in global ocean phytoplankton chlorophyll derived from 4 years of SeaWiFS measurements. *Global Biogeochem. Cycles*, **17**(4), 1112, doi: 10.1029/2002GB001942.

Young, D. K., and J. Kindle (1994): Physical processes affecting availability of dissolved silicate for diatom production in the Arabian Sea. *J. Geophys. Res.*, **99**, 22,619– 22,632.

Yusoff, F. M., T. Ichikawa, H. M. Matias and O. Azhar (2001): Total carbon, dissolved silica and chlorophyll *a* in the Straits of Malacca. p. 51-64. In *Aquatic Resource and Environmental Studies of the Straits of Malacca: Current Research and Reviews*, ed. by B. J. Sidik, A. Arshad, S. G. Tan, S. K. Daud, H. A. Jambari and S. Sugiyama, Malacca Straits Reseach and Development Centre (MASDEC), University Putra Malaysia, Serdang, Malaysia.